AZPH-TH/95–13 **PAR/LPTHE/95–24**

ENERGY DEPENDENCE OF STRANGE PARTICLE YIELDS FROM A QGP-FIREBALL

Jean Letessier[1], **Johann Rafelski**[2] and **Ahmed Tounsi**[1]

[1]Laboratoire de Physique Théorique et Hautes Energies*
Université Paris 7, 2 place Jussieu, F–75251 Cedex 05.

[2]Department of Physics, University of Arizona, Tucson, AZ 85721

Abstract

We explore, as function of the collision energy and stopping in relativistic nuclear collisions, the production yields of strange particles, in particular strange antibaryons, assuming formation of a deconfined thermal QGP-fireball which undergoes a sudden hadronisation. The non-equilibrium freeze-out conditions are established and strange antibaryon excitation functions are shown to have characteristic features that should allow to discriminate between the QGP hypothesis and other reaction scenarios.

PACS numbers: 25.75.+r, 12.38.Mh, 24.85.+p May/June 1995

*Unité associée au CNRS UA 280.

1 Introduction

In relativistic nuclear (A–A) collisions we search for a macroscopic, deconfined space time region in which soft quark and gluon degrees of freedom are present, the so-called quark-gluon plasma (QGP) — 'plasma' since it involves freely moving color charges within the limited reaction volume. Existence of this phase of matter seems to be an inescapable consequence of our theoretical knowledge about the fundamental hadronic interactions, qualitatively rooted in quantum chromo-dynamics (QCD). Nevertheless, it is important that we can demonstrate QGP formation experimentally, confirming the theoretical paradigm and permitting the experimental study of the strong interactions vacuum state.

Because of its rather limited (nuclear size) volume and hence very short lifespan [1] of about 4 fm/c, the study of the QGP phase is a formidable task. Moreover it is far from clear that this new phase can be formed and studied with the presently available nuclear beams, up to 200A GeV energy at CERN-SPS. However, we have shown in our recent work [2, 3] that strange particle production results point towards formation of the deconfined phase. In this paper we develop in full the method that involves as the observable strange antibaryons [4, 5]. Our primary interest is oriented towards (multiply) strange antibaryons for a number of reasons: the conventional backgrounds are small since the multi-step processes required occur relatively rarely in p–p interactions. Consequently, the relatively high production rate of multiply strange antibaryons in A–A reactions, and the central (in rapidity) spectral distribution, are indicative of a 'collective' formation mechanism. In the QGP reaction picture it is the ready made high density of (anti) strange quarks which leads to highly anomalous yields of multiply strange particles.

The use of specific hadronic particles in the search for QGP is only possible if the evolution of the final state is such that information about key properties of the primordial source is retained during the formation and evolution of the final state hadrons. This is observed experimentally indicating that there is no opportunity for the strange antibaryons emerging from deconfined state to re-equilibrate (annihilate) [2, 6], thus implying a sudden transition into the final hadronic particles [5, 6]. Of course it is far from certain today that QGP is formed already in the nuclear collisions below $\sqrt{s} = 10$A GeV. Several studies addressed recently the question [2, 7, 8, 9, 10] how the current data can distinguish between the formation of a central fireball consisting of a dense and very hot hadron (resonance) gas and the creation of a transient deconfined state such as the quark-gluon plasma (QGP) which subsequently hadronises. We note that even if this final state hadronisation involves a full re-equilibration, then the memory of the QGP should in some circumstance not be fully lost, since the deconfined state is often richer in entropy than the confined state [7, 11, 26, 13], which becomes visible as particle excess in the final state. Today, based on diverse results obtained at 200A GeV [2] it appears that we have a very favorable situation with the observable particles very much representing the expected properties of the primordial QGP state, while the results from BNL-AGS at 10-15A GeV are indicating that if QGP was formed, it has undergone a full re-equilibration transition [14]. Consequently, somewhere between the two energy regimes a major change in the reaction mechanism occurs. It appears to be of considerable importance to find in which energy range this change occurs and how other observables vary with energy in this changeover region.

Since the QGP picture works so well at 200A GeV, it is natural to expect that its formation is also occurring at somewhat lower energies. Therefore, within a dynamical collision model, using the equations of state (EoS) of QGP, we study in this paper how the thermal and chemical properties of the fireball of the dense hadronic matter change with energy. We predict here the production of strange particles as function of energy. Our primary goal is to find how the strange particle abundance in the final state is related to the conditions prevailing in the early moments of nuclear collisions. We develop an approach in which the collision force is counteracted by the thermal radiative pressure. The tacit assumption that we make is that the thermal equilibrium of quarks and gluons arises rapidly as a result of the primary interactions. This introduces without an explicit mechanism almost 70% of the final state entropy [15] — this is the excess QGP entropy [11] visible as the excess multiplicity of produced particles. Thus in our approach we do not resolve the important issue, what is the energy and more generally the conditions required in the collision for the formation of the deconfined state. On the other hand, the principal virtue of the thermal model framework adopted here is that the spectra and particle abundances can be described in terms of a few parameters which have simple physical meaning.

Aside of the rather demanding multi-strange antibaryon signature of the QGP, there is the more readily available, but less specific overall abundance of strangeness. Strange particle signatures of dense baryon rich hadronic matter have been theoretically considered for nearly two decades [16]. Because of the intrinsic difficulties related to the detection of strange particles within the large multiplicity of hadrons produced in relativistic nuclear collisions only recently results have been presented which allow a test of the different theoretical models (for a recent review of available results, see Ref. [17]). Because strangeness production processes constitute a bottleneck in chemical equilibration of conventional confined strongly interacting matter [18, 19, 20, 16], strangeness production in QGP has been widely studied [4, 18, 19, 21]. In the theoretical description several microscopic features combine to produce this enhancement: there is a high quark-gluon density and the production threshold of strange quark pairs in QGP is below the mean energy (temperature) of the constituents present. The computed strangeness relaxation time constant $\tau_{\rm s} \leq 6$ fm/c towards the attainment of the strange phase space equilibrium abundance in the QGP phase is of the magnitude similar to the estimated lifespan $\tau_{\rm QGP} \simeq R/c$ of the dense QGP state, where R is the characteristic size parameter of the QGP phase. Consequently, even if the magnitude of both these time constants is still rather uncertain, their similarity is of considerable importance for the exploration of the QGP phase: varying the size of the colliding nuclei, or the mean impact parameter in collision, we can change the size R of the interaction region and thus change the lifespan of the dense state. Since $\tau_{\rm s}$ depends primarily on the temperature (mean glue energy), we could explore how this impacts the strangeness chemical equilibration and compare with the theoretical predictions.

A crucial confirmation of the reaction picture would arise if the changes observed in the chemical equilibration of strangeness would be equally attainable when the energy content in collision is varied. More importantly, this could be done at the maximum volume available, thus assuring that unwanted dynamical variations such as changes in longitudinal flow (transparency) with changes in impact parameter were minimal, while the highest accessible particle and energy density is explored in each case. For the strange antibaryon signature

this approach is much preferred, as the abundance of particles produced, and their centrality remains assured. Since the (enhanced) production of (multi)strange antibaryons is widely considered to be more specifically related to the deconfinement than the strangeness enhancement in general, it would be of considerable importance to obtain data on (multi)strange antibaryon production as function of energy.

Within our approach one of key tacit assumptions is that there is formation at central rapidity of an energy and baryon-rich, fireball. We believe that the pattern of diverse particle production processes confirms the view that even the 200A GeV collisions are leading to the formation of a domain of space-time in which not only energy, but also considerable baryon number is present. For example, the rapidity distribution of Λ and $\overline{\Lambda}$ as measured by the NA35 experiment [22] affirms such a picture of the A–A reactions. These results show that the S–Ag/W/Pb and even the S–S collisions at 200A GeV are far from the limit of baryon-transparency in which the valence quarks of projectile and target are presumed to leave the central rapidity region [23]. Relatively large stopping behavior at 200A GeV could be expected: assuming that a valence quark carries, in a typical case, about 1/6 of the energy of a nucleon, and placing the observer in the CM frame, we find that we would have two 1.5 GeV partons colliding at CERN-SPS energies — at BNL-AGS energies (10-15A GeV) a head-on collision interpreted in this picture would occur between partons of 0.4 GeV. Moreover, we have in each hadron a rather wide distribution of parton energies, and thus many collisions between sea and valence partons are occurring at still considerably lower energies. Just a few elastic or inelastic interactions will suffice to stop many partons in the central fireball. It is thus not surprising that in the particle spectra there is little room, if any, for the separation in rapidity of energy and baryon number.

In this consideration it is important to remember that the more easily analyzed and understood symmetric A–A collisions at small impact parameters the surface (corona) nucleons will undergo interactions which resembles the normal p–p collision environment. These p–p like components should not be confused with the more specific elements of the A–A interactions — strange particles are a good tag on these specific interactions, since strangeness production in A–A collisions is enhanced compared to p–p and p–A based expectations, and because there are a number of particles (such as $\overline{\Lambda}$) which are rather rarely produced in p–p collisions, in contrast to A–A interactions, and which show, very strongly in these interactions, features we would interpret as originating in the central fireball.

Our paper is organized as follows: in next section 2 we explore the conditions reached in the early deconfined QGP fireball formed e.g. in the CERN-SPS collisions. We then compare in section 3 the results we obtain with those derived for the S–W/Pb at CERN-SPS and Au–Au interactions at BNL-AGS. We obtain an excellent agreement with all the available data. We also make predictions about strange particle production for the forthcoming round of experiments and about the expected particle yield behavior as the energy of the collision is varied.

2 Properties of the QGP State

2.1 The Thermal Approach

Application of the thermal model to hadronic processes implies that on the prevailing time scale of the interaction, thermalization of the relevant degrees of freedom is rapid. This means that thermal features are seen in the particle production processes [24] which are not rooted directly in the microscopic features of strong interactions (QCD). We can expect that the leading particle and flow effects diminish in their significance as the size of the interaction region increase. Thus soft hadronic physics in the A–A case should be easier to understand. The original motivation to study these large nuclei in highly relativistic collisions was just the hope that we will unravel the soft hadronic physics which has remained in veil when studied with the p–p interactions.

It is convenient to incorporate in the model development the particle spectra as function of the rapidity y and transverse mass $m_\perp$ of a particle

$$y = \frac{1}{2}\ln\left(\frac{E+p_z}{E-p_z}\right), \qquad E = m_\perp \cosh y\,, \qquad m_\perp = \sqrt{m^2+p_\perp^2}\,, \tag{1}$$

where '$\perp$' is perpendicular to the collision axis 'z'. While $m_\perp$ is invariant under Lorenz transformations along the collision axis, the particle rapidity y is additive, that is it changes by the constant value of the transformation for all particles. This allows to choose the suitable (CM — center of momentum) reference frame characterized by its rapidity $y_{\rm CM}$ for the study of the particle spectra.

The 'thermal' hypothesis presupposes that the shape of these spectra is sufficiently similar to allow a reduction of all data to just one 'Boltzmann' spectral shape centered around the fireball rapidity $y_{\rm CM}$:

$$\frac{dN}{d^3p} = N_i e^{-E^{(i)}/T} = N_i e^{-\cosh(y-y_{\rm CM})\,m_\perp^i/T}\,. \tag{2}$$

The parameters of each particle distribution [25] include the inverse slope T ('temperature') of the $m_\perp$ distribution, centered around the $y_{\rm CM}$. In particular the temperature T derived from the transverse mass distribution should be common for all types of particles produced by the same thermal mechanism. This relates many particle spectra to each other and reduces the number of observables considerably. Similarly, $y_{\rm CM}$ should be also the same for different particles originating in the same thermal source. In addition, for each particle there is the normalization constant N_i. We will discuss below how these constants are determined by a chemical equilibrium parameters, aside of the volume V. Let us note in passing that the presence of a common inverse slope parameter for different particle spectra, which is different from the one found in p–p collisions is well established experimentally. For example, for the 200A GeV S–W/Pb interactions the inverse slope parameters of strange baryons and antibaryons [27] and for example of high $m_\perp$ neutral mesons [28] are all consistent with $T = 232$ MeV.

Since a wealth of experimental data can be described with just a few model parameters, this leaves within the thermal model a considerable predictive power and a strong check of the internal consistency of thermal approach. Specifically, in the directly hadronising off-equilibrium QGP-fireball model [2] there are 4 parameters (aside of T and $y_{\rm CM}$)

characterizing all particle spectra: two fugacities $\lambda_{\rm q}$, $\lambda_{\rm s}$, and two particle abundance non-equilibrium parameters, the strangeness occupancy factor $\gamma_{\rm s}$ and the ratio $R_c^{\rm s}$ related to meson and baryon abundances (see section 3.2). Moreover, these physical parameters can be determined using a dynamical picture of the collision, in which the input is derived from more general qualitative conditions of the colliding system, such as the energy content or stopping power. Thus the validity of thermal and chemical equilibrium can be conclusively tested, comparing the predicted particle spectra and yields with theoretical predictions without the need or capability to modify and adapt the description to each new result which is reported.

2.2 Parameters of the Fireball

We now introduce and discuss in qualitative terms the model parameters and their temporal evolution during nuclear collision. Practically all results we will obtain will hinge on the time evolution scenario we adopt. At the present time the experimental constraints are not limiting our reaction and evolution picture in a unique way. The picture we adopt is in qualitative, and as we shall see, also in quantitative agreement with a number of important experimental results, and it is in accord with the general properties of the strong interactions and hadronic structure widely known and accepted today.

2.2.1 Temporal Evolution of the Fireball

We suppose that the relevant time development stages of the relativistic nuclear collision comprise:

1. The pre-thermal stage lasting perhaps 0.2–0.4 fm/c, during which the thermalization of the initial quark-gluon distributions occur. During this time most of the entropy obtained in the collision must be created by mechanisms that are not yet understood — this is also alluded to as the period of de-coherence of the quantum collision system. Our lack of understanding of this stage will not impact our results, as the reason that we lack in understanding is that the hadronic interactions erase the memory of this primordial stage.

2. The subsequent inter-penetration of the projectile and the target lasting about ~ 1 fm/c, probably also corresponding to the time required to reach chemical equilibrium of gluons G and light non-strange quarks $q = u,\, d$.

3. A third time period (3–5 fm/c) during which the production and chemical equilibration of strange quarks takes place. During this stage many of the physical observables studied here will be initiated.

4. Hadronisation of the deconfined state ensues: it is believed that the fireball first expands at constant specific entropy per baryon, and that during this evolution or at its end it decomposes into the final state hadrons, under certain conditions in a (explosive) process that does not allow for re-equilibration of the final state particles.

In the sudden hadronisation picture of the QGP fireball suggested by certain features seen in the analysis of the strange antibaryon abundances for the 200A GeV nuclear collision data [2, 3, 6], the hadronic observables we study are not overly sensitive to the details of stage *4*. Akin to the processes of direct emission, in which strange particles are made in recombination–fragmentation processes [5], the chemical conditions prevailing in the deconfined phase are determining many relative final particle yields. If the hadronisation occurs as suggested by recent lattice results [29] at a relatively low temperature (e.g. 150 MeV), the total meson abundance which is governed by the entropy content at freeze-out of the particles, is found about 100% above the hadronic gas equilibrium expectations [11]. This is consistent with the source of these particles being the QGP [11, 2]. The freeze-out entropy originates at early time in collision since aside of strangeness production which is responsible for about 10% additional entropy there is no significant entropy production after the initial state has occurred [11]. Similarly, the relatively small thermal abundance of baryons must be enhanced by the factor 5 in order to maintain a ratio $R_c^{\rm s} = 0.4$ [2].

On the other hand the experimental results obtained at 15A GeV are consistent with the thermal equilibrium hadronic gas state expectations [14]. In the event that the source of these particles should indeed be a QGP fireball, a slow re-equilibration transition should be envisaged here. In this scenario the details of hadronisation mechanisms are of even lesser relevance since the equilibrium state is reached among the final hadron gas particles.

2.2.2 Temperature

During the initial contact of the two nuclei, as soon as stage *1* is reached, it is likely that the most extreme conditions (highest temperature) prevails. Subsequently, temperature decreases rapidly, primarily due to two mechanisms: there is rapid quark and gluon production, leading towards the chemical equilibration, and second, the fireball expansion/emission cooling occurs. We will account for these two effects balancing energy per baryon or entropy per baryon of the fireball as appropriate for the evolution stage. In this way, we implement during the stage *2* a one dimensional, hydrodynamical evolution of the dense deconfined hadronic matter, in addition allowing for the approach to chemical equilibrium. We encounter a considerable drop in temperature between the initial stage *1* and the final state *4* freeze-out point, but the entropy content which determines the final particle multiplicities remains nearly constant: aside of the initial state entropy formation all the additional increase is due to the formation of the strangeness flavor.

The different stages of the evolution are characterized by the temperatures:

$T_{\rm th}$ temperature associated with initial thermal equilibrium,
$\downarrow$ *production of* q, $\bar{q}$, G, *expansion;*
$T_{\rm ch}$ temperature of chemical equilibrium for non-strange quarks and gluons,
$\downarrow$ *production of* s, $\bar{s}$ *quarks and fireball expansion;*
T_0 temperature of maximal chemical equilibrium: 'visible' temperature,
$\downarrow$ *fireball expansion/particle radiation*;
$T_{\rm f,s}$ temperature at freeze-out for non-strange and strange particles,

with obviously $T_{\rm th} > T_{\rm ch} > T_0 \geq T_{\rm f}$.

In the transverse mass spectra of strange (anti)baryons a temperature $T_\perp$ is found. If the final state particles emerge directly without re-equilibration from the fireball [5, 6], this observed temperature ($T_\perp = 232 \pm 5$ in S–A collisions at 200A GeV) in the particle spectra would be closely related to the full chemical equilibration temperature T_0 : subsequent to the establishment of the conditions at T_0 we have either directly the emission of particles and thus we have $T_\perp \leq T_0$, or there is collective, (so called transverse) radial flow in the hot matter, in which fraction of the thermal energy is converted into the flow energy. When the final state particles emerge from the flowing surface, they are blue-shifted by the flow velocity. This Doppler shift effect restores the high apparent T_0 in high $m_\perp$ particle spectra [30]:

$$T_\perp \leq T_0 \equiv \sqrt{\frac{1+v_{\rm f}}{1-v_{\rm f}}} T_{\rm f}\,, \qquad T_\perp \leq T_0 \equiv \sqrt{\frac{1+v_{\rm s}}{1-v_{\rm s}}} T_{\rm s}\,; \tag{3}$$

— strange and non-strange particles may not originate in exactly the same condition and hence we introduced here the option to have different freeze-out temperature. In view of the smaller strange particle cross sections we expect $T_{\rm s} \geq T_{\rm f}$.

As suggested in Eq. (3), the temperature T_0 at the onset of flow is close to the inverse slope spectral temperature $T_\perp$ implied by the high $m_\perp$ (strange antibaryon) particle spectra. Despite our ignorance of the freeze-out mechanisms and conditions, we believe that the uncertainty in the value of the initial temperature as derived from the value of $T_\perp$ in Eq. 3 is not large. If QGP phase is directly dissociating by particle emission, this is trivially so. If there were to be substantial flow, one can assume some temperature T_0, and given the EoS, compute accurately the hydrodynamic radial expansion [1]; at the high $m_\perp \simeq 2$ GeV considered here, using Eq. (3) we find that the inverse slope $T_\perp$ of the particle distributions is equal or a bit smaller than T_0.

2.2.3 Fireball Rapidity

The fireball is created in central symmetric collisions at the CM-rapidity of the N–N system, which is for relativistic systems just is 1/2 of the projectile rapidity. For asymmetric collisions such as S–Au/W/Pb the CM rapidity depends on the ratio of the participating masses of the projectile $A_{\rm P}$ and target $A_{\rm T}$ nuclei. The center of momentum frame is [31] (neglecting small corrections):

$$y_{\rm CM} = \frac{y_{\rm P}}{2} - \frac{1}{2} \ln \frac{A_{\rm T}}{A_{\rm P}}\,. \tag{4}$$

Assuming small impact parameter collisions with a suitable central trigger, all projectile nucleons participate while the target participants $A_{\rm T}$ can be estimated from a geometric 'interacting tube' model [31]. This model reproduces well the central value of rapidity center particle spectra in the specific case of 200A GeV S–Au/W/Pb interactions. One in particular finds $y_{\rm CM} = 2.6 \pm 0.1$, the uncertainty arising from the impact parameter averaging and variations of the surface nucleon participation. Once the central rapidity is defined, and the ratio of participating projectile and target masses is known, it is possible to determine the CM-energy involved in the interaction. It is from this simple kinematic considerations that we derive the energy values presented below in section 2.4.

2.2.4 Particle Fugacities

Among the chemical (particle abundance) parameters there are the well known particle fugacities, which allow to conserve flavor quantum numbers. Three fugacities are introduced since the flavors u, d, and s are separately conserved on the time scale of hadronic collisions and can only be produced or annihilated in particle-antiparticle pair production processes[1].

The fugacity of each hadronic particle species is the product of the valence quark fugacities, thus, for example, the hyperons have the fugacity $\lambda_{\rm Y} = \lambda_{\rm u}\lambda_{\rm d}\lambda_{\rm s}$. Fugacities are related to the chemical potentials μ_i by:

$$\lambda_i = e^{\mu_i/T}\,, \quad \lambda_{\bar{\imath}} = \lambda_i^{-1} \qquad i = u,\, d,\, s\,. \tag{5}$$

Therefore, the chemical potentials for particles and antiparticles are opposite to each other, provided that there is complete chemical equilibrium, and if not, that the deviation from the full phase space occupancy is accounted for by introducing a non-equilibrium chemical parameter γ (see below).

2.2.5 Phase Space Occupancy

Thermal and chemical equilibria are two very different phenomena. In general, the production of particles is a considerably slower process than elastic hadronic collisions, and thus even if we assume in our work a thermal equilibrium scheme, we should not expect the chemical equilibrium to be present. In addition, there is the relative and absolute chemical equilibrium. In the former, the particle abundances are in relative equilibrium with each other, in the latter the total particle yields are just filling the full available phase space — relative chemical equilibrium is in general easier to attain than the absolute chemical equilibrium. Our picture of rapid QGP fireball disintegration in which no equilibration takes place in the final state, implies that chemical (abundance) non-equilibrium features should be present in the final state.

Strangeness flavor provides an interesting example of the above. Calculations [18, 21] of the chemical relaxation constant show that in general it will not fully saturated the available phase-space. Therefore, we need to introduce the associated off-equilibrium parameter $\gamma_{\rm s}$. Since the thermal equilibrium is, as discussed above, established within a considerably shorter time scale than the (absolute) chemical equilibration of strangeness, we can characterize the saturation of the strangeness phase space by an average over the momentum distribution:

$$\gamma_{\rm s}(t) \equiv \frac{\int d^3p\, d^3x\, n_{\rm s}(\vec{p},\vec{x};t)}{\int d^3p\, d^3x n_{\rm s}^{\infty}(\vec{p},\vec{x})}\,, \tag{6}$$

where $n_{\rm s}^{\infty}$ is the equilibrium particle density. The factor $\gamma_{\rm s}$ thus enters the phase space momentum Boltzmann distribution as a multiplicative factor, and with the $\vec{x}$ dependence contained solely in the statistical parameters we have:

$$n_{\rm s}(\vec{p},\vec{x};t) \simeq \gamma_{\rm s}(t) n_{\rm s}^{\infty}(\vec{p};T(\vec{x},t),\mu_{\rm s}(\vec{x},t))\,. \tag{7}$$

[1]In many applications it is sufficient to combine the light quarks into one fugacity $\lambda_{\rm q}^2 \equiv \lambda_{\rm d}\lambda_{\rm u}$, $\mu_{\rm q} = (\mu_{\rm u}+\mu_{\rm d})/2$. The slight asymmetry in the number of u and d quarks is described by the small quantity $\delta\mu = \mu_{\rm d} - \mu_{\rm u}$, which may be estimated by theoretical considerations [2].

A further refinement should be noted: when the quantum aspects of the particle distributions are incorporated and the maximum entropy state of an isolated physical system (closed system) is obtained, the absolute chemical equilibrium coefficients γ_i enter as multiplicative coefficients in front of the Boltzmann factor within the quantum Bose/Fermi distribution [15]:

$$n_i^{\mathrm{B,F}} = \frac{1}{\gamma_i^{-1}\lambda_i \mathrm{e}^{\beta\epsilon_i} \mp 1}\,, \tag{8}$$

along with the fugacity factors .

The final freeze-out value of γ_{s} is a parameter which impacts the particle ratios in a two fold way: there is the simple proportionality (in the Boltzmann limit) of the particle yields to γ_{s}^n, — where n is the number of strange quarks contained in the hadron considered, and furthermore, the value of γ_{s} impacts the cooling that the fireball undergoes to produce strangeness. Unexpectedly, it is rather straightforward to extract from the strange antibaryon experimental particle yields [6, 2, 3, 10] the value of γ_{s}. Roughly speaking, γ_{s} makes its appearance in all particle ratios in which we compare the abundances involving different strangeness content. The measurement of γ_{s} is thus an important step towards the understanding of the behavior of highly excited hadronic phases: γ_{s} can be studied varying a number of parameters of the collision, such as the volume occupied by the fireball (varying size of the colliding nuclei and impact parameter), the trigger condition (e.g. the inelasticity), the energy of colliding nuclei when searching for the threshold energy of abundant strangeness formation.

The theoretical dynamical model to investigate $\gamma_{\mathrm{s}}(t)$ has been developed to considerable detail [32, 33] — it arises from a standard population evolution equation and its interplay with the expansion-dilution-dissociation of the fireball. For a QGP state with its fast gluonic strangeness production even the natural short fireball lifetime of only a few fm/c should be nearly sufficient to reach values of $\gamma_{\mathrm{s}} \simeq 1$. Detailed balance assures that the production and annihilation processes are balancing each other as $\gamma_{\mathrm{s}} \to 1$. At large times the approach to equilibrium takes the form

$$1 - \gamma_{\mathrm{s}} \to e^{-t/\tau_{\mathrm{s}}}, \qquad t \gg \tau_{\mathrm{s}}\,, \tag{9}$$

where τ_{s} is the relaxation time for strangeness equilibration which can be computed using standard QCD methods. A recent evaluation of this work [21] confirmed that the glue fusion processes [18] are dominating the strangeness production rates in QGP, with $\tau_{\mathrm{s}} \simeq 2$ fm/c for the here relevant $T \simeq 250$ MeV temperature range. The experimental results yield $\gamma_{\mathrm{s}} = 0.7$–$1$, imply according to Eq. (9) a lifespan of the the plasma state to be greater than 3 fm.

In a purely HG fireball, with its expected much longer strangeness saturation time scale, small values of $\gamma_{\mathrm{s}} \sim 0.1$ like those extracted from N–N collisions should prevail [20]. A measurement of γ_{s} thus in principle provides important information on the strangeness production time scale and hence a relatively large value of γ_{s} requires some new physics feature in the structure of the collision fireball, which we like to associate with QGP formation.

2.3 QGP Equations of State

The partition function of the interacting quark-gluon phase can be written as:

$$\ln Z^{\mathrm{QGP}} = \sum_{i\in \mathrm{QGP}} \frac{g_i(\alpha_s)V}{2\pi^2} \int \pm \ln\left(1 \pm \gamma_i \lambda_i e^{-\sqrt{m_i^2(T)+p^2}/T}\right) p^2\, dp\,, \tag{10}$$

where $i = G,\ q,\ \bar{q},\ s,\ \bar{s}$, with $\lambda_{\bar{i}} = \lambda_i^{-1}$ and $\gamma_{\bar{i}} = \gamma_i$. We take into account the QCD interaction between quarks and gluons by allowing for thermal masses

$$m_i^2(T) = (m_i^0)^2 + (c\,T)^2\,. \tag{11}$$

For the current quark masses we take:

$$m_{\mathrm{q}}^0 = 5 \text{ MeV}, \quad m_{\mathrm{s}}^0 = 160 \text{ MeV}, \quad m_{\mathrm{G}}^0 = 0\,.$$

We have $c^2 \propto \alpha_{\mathrm{s}}$, α_s being the QCD coupling constant. Considering the theoretical uncertainty regarding the coefficient $c(\alpha_{\mathrm{s}})$, we explored two different approaches:

1. We fix $c = 2$, arising for $\alpha_s \sim 1$ (the exact value was not of essence), and allowing for another effect of the QCD-interaction, the reduction of the number of effectively available degrees of freedom. We implement the following effective counting of gluon and quark degrees of freedom, motivated by the perturbative QCD formulæ:

$$\begin{aligned} g_{\mathrm{G}} &= 16 \ \rightarrow \ g_{\mathrm{G}}(\alpha_s) = 16\left(1 - \frac{15\alpha_s}{4\pi}\right), \\ g_{i-\mathrm{T}} &= 6 \ \rightarrow \ g_{i-\mathrm{T}}(\alpha_s) = 6\left(1 - \frac{50\alpha_s}{21\pi}\right), \\ g_{i-\mathrm{B}} &= 6 \ \rightarrow \ g_{i-\mathrm{B}}(\alpha_s) = 6\left(1 - 2\frac{\alpha_s}{\pi}\right), \end{aligned} \tag{12}$$

   where $i = u,\ d,\ s$. In Eq. (12) two factors are needed for quarks: the factor $g_{i-\mathrm{T}}$ controls the expression when all chemical potentials vanish (the T^4 term in the partition function for massless quarks) while $g_{i-\mathrm{B}}$ is taken as coefficient of the additional terms which arise in presence of chemical potentials. We took $\alpha_s = 0.6$ which turned out to be the value best suited for the experimental data points[2].

2. A fit proposed by Kämpfer et al. [34, 35] made to the lattice data for the SU(3) gauge sector and extended to quarks

$$c^2 = 3.8\alpha_s^{\mathrm{m}}(T)\,; \tag{13}$$

$$\alpha_s^{\mathrm{m}}(T) = \frac{4\pi}{9\ln(T/T_c + 0.023)^2}\,, \tag{14}$$

   where the form of α_s^{m} is motivated by $\alpha_s(q^2)$. The critical temperature of the QGP transition to confined phase is chosen at $T_c = 150$ MeV and the infrared cutoff at $0.023T_c$.

[2]This value arises at $T = 2.2\,T_c$ in the fit [34, 35] to lattice gauge data without quarks.

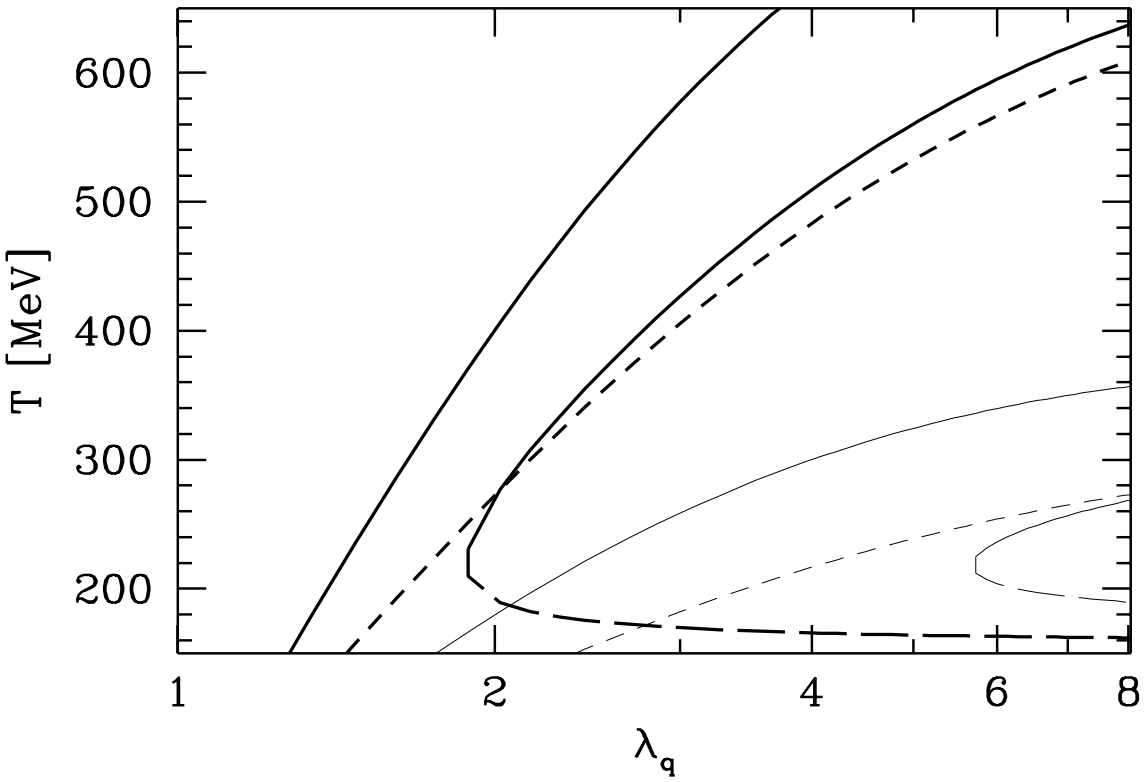

Figure 1: Properties of different QGP-EoS: constraint between temperature T and light quark fugacity $\lambda_{\rm q}$ for a given energy content per baryon $E/B = 4.3$ (thin lines) and 9.6 GeV (thick lines). Upper solid line: procedure *1* of EoS (see text), lower solid lines joining onto the long-dashed lines (second solution branch): procedure *2* EoS and short-dotted: free quark-gluon gas.

The main difference between these two approaches is how the quark and gluon degrees of freedom are suppressed near to the critical temperature. In both cases these phenomenologically motivated procedures are a bold extension of the established perturbative and/or lattice QCD results.

Given these interaction effects, the Bose/Fermi distributions for quarks/gluons, Eq. (10), allow us to obtain in a consistent way any physical property of this model EoS of the QGP phase. These are shown in Fig. 1. We show here in T–λ_q domain lines of fixed energy per baryon (thick lines: 9.6 GeV, thin lines 4.3 GeV) — solid lines are for the procedure *1*, dashed lines are the ideal gas (no interaction) lines, long dashed is the second solution branch of the procedure *2*, which attaches to the primary solution branch also shown as solid lines. Note that the second solution branch is probably an artifact, as it tangents the critical temperature, where this method is questionable. Interestingly, we note that at high T the perturbative result is just below the results of procedure *2*, indicating that the change in energy density and baryon number density due to thermal masses is equal, and thus the ratio is similar to the free gas result. There is substantial difference between the procedure *1* and the free gas, which originates in different changes of the degrees of freedom due to perturbative interactions in the dominant terms of energy density and baryon density.

This representation of the ratio of two densities amplifies the impact of interactions and shows how these are incorporated in the different approaches. We see that while in the procedure *2* fitted to lattice data the treatment of the energy density is particularly accurate for baryon-less plasma, for finite baryon density of interest here the results are of definitively questionable validity. In particular, near to the critical temperature (taken here to be $T_c = 150$ MeV) the large thermal mass of quarks eliminates the baryon density effectively and thus it is not even possible to find for a given ratio of energy density to baryon density a reasonable solution for $T \sim T_c$ while for 'high' T essentially the free quark-gluon gas result is reproduced.

Since our present work is primarily concerned with the baryon density dependence of the diverse observables near to T_c, presumably $T_c < T < 2T_c$ and $\mu_q \simeq T$, it is clear that we cannot use the model *2* without prior major theoretical improvements applicable to high baryon density domain, such as is the inclusion of the chemical potential dependence in α_s and in the thermal masses, and for fermions, the effect of Fermi blocking on the polarization function. We thus assume the procedure *1* with parameters as described above.

2.4 Energy Content in the Fireball

We now commence the evaluation of the initial conditions reached in the collision: an important constraint arises from the energy per baryon content in the fireball. The considerations of the previous section allow to relate a given energy per baryon[3] E/B to the statistical parameters T and $\lambda_{\rm q}$. On the other hand, the collision energy gives

$$\frac{E}{B} = \frac{\eta_{\rm E} E_{\rm CM}}{\eta_{\rm B} A_{\rm part}} \simeq \frac{E_{\rm CM}}{A_{\rm part}}, \tag{15}$$

where $A_{\rm part}$ is the number of nucleons participating in the reaction. The last equality follows when the stopping fractions are equal — the experimental particle spectra we are addressing here, and in particular the visible presence of baryons in the central rapidity region, are implying that this is a reasonable assumption for the current experimental domain. In consequence, the energy per baryon in the fireball is to be taken as being equal to the kinematic energy available in the collision. In the current experiments we have the following kinematic energy content:

$$\begin{array}{lcl}
\text{Au–Au at 10.5A GeV} & \rightarrow & E/B = 2.3 \text{ GeV} , \\
\text{Si–Au at 14.6A GeV} & \rightarrow & E/B = 2.6 \text{ GeV}, \\
\text{A–A at 40A GeV} & \rightarrow & E/B = 4.3 \text{ GeV}, \\
\text{Pb–Pb at 158A GeV} & \rightarrow & E/B = 8.6 \text{ GeV}, \\
\text{S–W/Pb at 200A GeV} & \rightarrow & E/B = 8.8 \text{ GeV} , \\
\text{S–S at 200A GeV} & \rightarrow & E/B = 9.6 \text{ GeV} ,
\end{array}$$

Note that above we assumed collision with the geometric target tube of matter when the projectile is smaller than the target, see section 2.2. The specific energy content E/B, given EoS, establishes a constraint between the thermal parameters. In Fig. 2 we show in the T–$\lambda_{\rm q}$

[3]Here B is the baryon number. To avoid confusion the bag constant is denoted $\mathcal{B}$.

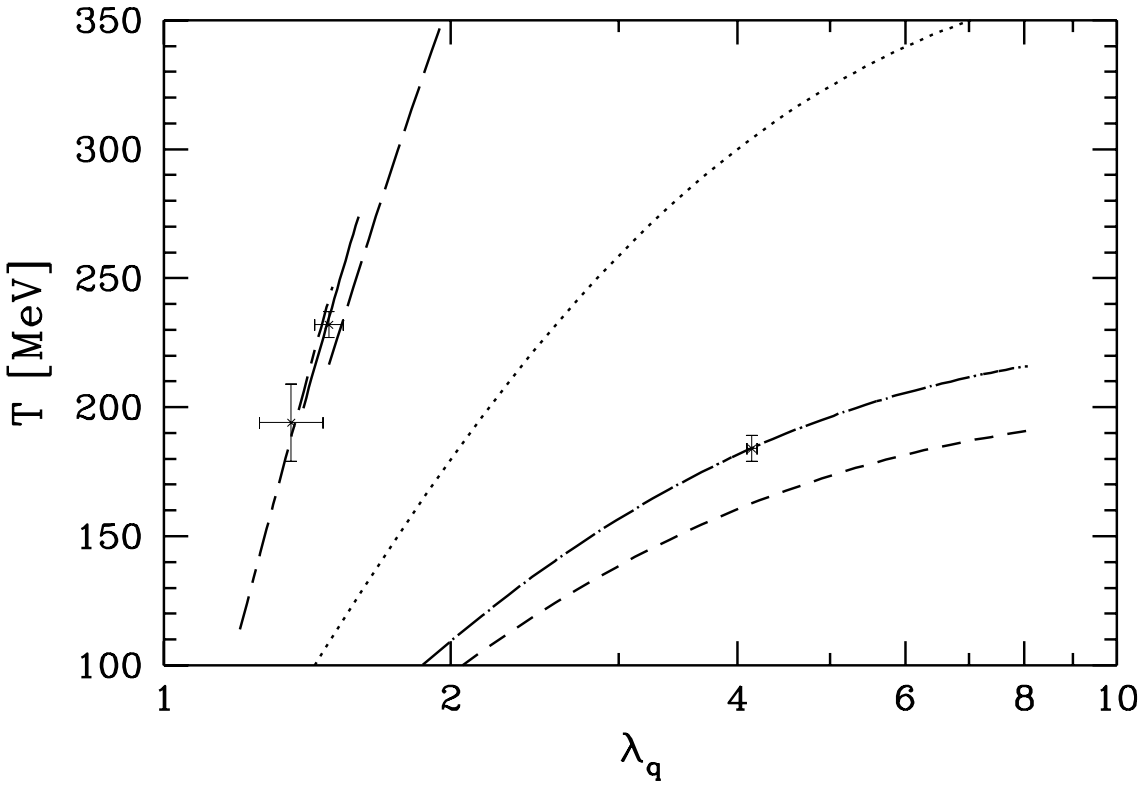

Figure 2: QGP-EoS according to procedure *1* constraint between temperature T and light quark fugacity λ_q for a given fireball energy content per baryon E/B appropriate for the BNL-AGS and CERN-SPS collision systems. Left to right: 2.3 (Au–Au), 2.6 (Si–Au), 4.3 (A–A), 8.6 (Pb–Pb), 8.8 (S–PB/W) and 9.6 (S–S) GeV. See text for a discussion of experimental points.

plane the lines corresponding to the constraint on the QGP-EoS according to procedure *1*, see section 2.3, arising from fixing the energy per baryon at kinematic value listed above (rising from bottom right to left). In the middle we show the lowest CERN-SPS accessible energy, 4.3 GeV, which bridges the current CERN-SPS domain shown to the left to the BNL region on the lower right. The experimental crosses show the values of λ_q arising in our data analysis [2, 3, 14], combined with the inverse slopes temperatures, see section 2.2, extracted from transverse mass particle spectra. The fact that the experimental results fall on the lines shown in Fig. 2 is primarily due to the choice $\alpha_s = 0.6$ — as this is the usual value in this regime of energy it implies for a QGP fireball EoS hypothesis that the assumption that stopping of energy and baryon number is similar deserves further consideration.

2.5 Pressure Balance

We have seen that the QGP energy per baryon constraint between λ_q and T (see Fig. 2) allows for a good agreement with experiment [38]. There remains the issue what physical constraint or principle determines which of the possible pair of T, λ_q values along the individual curves in Fig. 2 is experimentally recorded by the cross shown. We have explored the properties of the QGP phase along these lines of constant energy per baryon and have noticed that

with increasing T the pressure in the QGP phase increases, and that the experimental points coincide with the dynamical pressure generated in the collision. This confirms the intuitive idea that the initial conditions reached in the central fireball arise from the equilibrium between the fireball internal thermal and external compression pressure.

This condition takes the form [36]:

$$P_{\rm th}(T,\lambda_i,\gamma_i) = P_{\rm dyn} + P_{\rm vac}\,. \tag{16}$$

The thermal pressure follows in usual way from the partition function

$$P_{\rm th} = T/V \ln Z\,, \tag{17}$$

where aside of the temperature T, we encounter the different (quark and gluon) fugacities λ_i and the chemical saturation factors γ_i for each particle. For the vacuum pressure we will use:

$$P_{\rm vac} \equiv \mathcal{B} \simeq 0.1{\rm GeV/fm}^3\,. \tag{18}$$

The pressure due to kinetic motion follows from well-established principles, and can be directly inferred from the pressure tensor [37]:

$$T^{ij}(x) = \int p^i u^j f(x,p){\rm d}^3p\,, \quad i,j = 1,2,3\,. \tag{19}$$

We take for the phase-space distribution of colliding projectile and target nuclei

$$f_{\rm P,T}(x,p) = \rho_{\rm P,T}(x)\delta^3(\vec{p} \pm \vec{p}_{\rm CM})\,, \tag{20}$$

and hence in Eq. (19) $u^j = \pm p^j_{\rm CM}/E_{\rm CM}$. We assume that the nuclear density is uniform within the nuclear size, $\rho_0 = 0.16$ /fm^3.

To obtain the pressure exerted by the flow of colliding matter, we consider the pressure component T^{jj}, with j being the direction of $\vec{v}_{\rm CM}$. This gives

$$P_{\rm dyn} = \eta_{\rm p}\rho_0 \frac{p^2_{\rm CM}}{E_{\rm CM}}\,. \tag{21}$$

Here it is understood that the energy $E_{\rm CM}$ and the momentum $p_{\rm CM}$ are given in the nucleon–nucleon CM frame and $\eta_{\rm p}$ is the momentum stopping fraction — only this fraction $0 \leq \eta_{\rm p} \leq 1$ of the incident CM momentum can be used by a particle incident on the central fireball (the balance remains in the un-stopped longitudinal motion) in order to exert dynamical pressure. For a target transparent to the incoming flow, there would obviously be no pressure exerted. In Fig. 3 we show, as function of momentum stopping $\eta_{\rm p}$ the collision pressure P. For $\eta_{\rm p} \simeq 0.5$ the value of the pressure P is close to the value found in the QGP phase (see table 1). We note that if indeed in Pb–Pb collisions the momentum stopping increases, the dynamical pressure can double, causing a considerable increase in the baryon compression and the associated slow rise of $\lambda_{\rm q}$ as the size of the collision system increases.

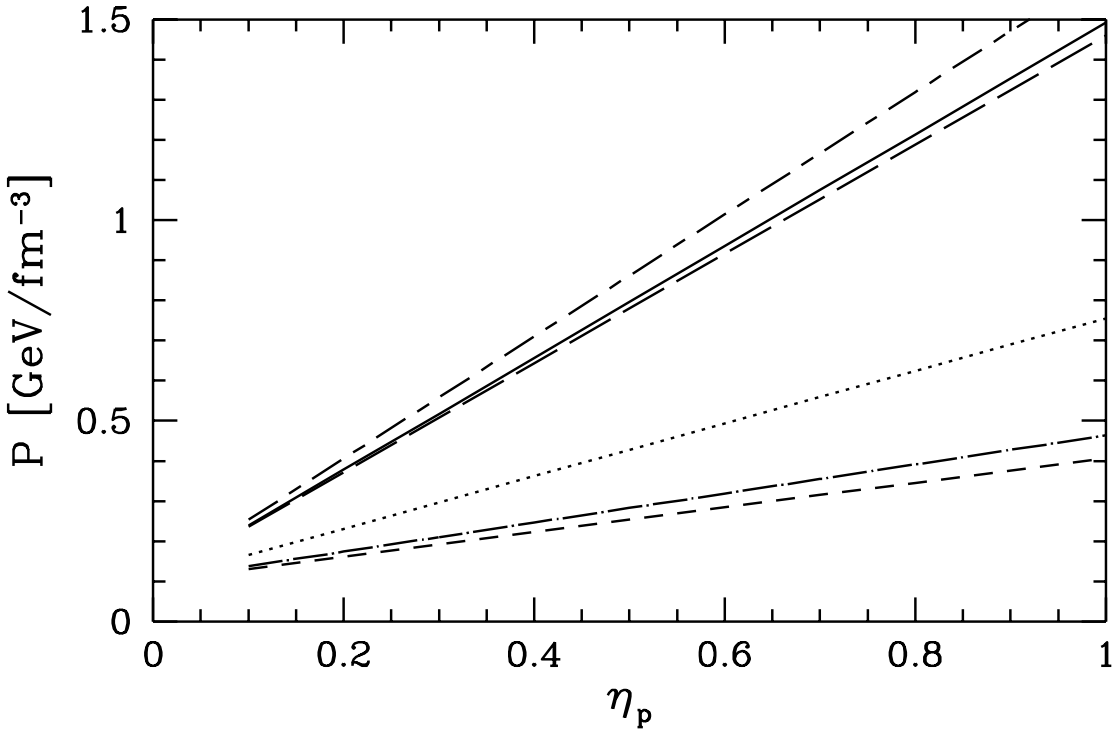

Figure 3: The collision pressure P as function of momentum stopping $\eta_{\rm p}$ for different values of E/B — 2.3, 2.6, 4.3, 8.6, 8.8 and 9.6 GeV (from bottom to top, solid line is for 8.8 GeV).

2.6 Final State Statistical Parameters

We are here primarily interested in determining the properties of the (near) chemical equilibrium state of the QGP-fireball prior to its disintegration. During the time the nuclei interact in collision, we assume rapid thermal equilibration of the fraction η of the kinetic energy. The evolution of particle numbers towards chemical equilibrium occurs in this stage under the constraint of a given constant (compression-)pressure and energy per baryon. Given values of $E_{\rm CM}$ and $\eta_{\rm p}$, as well as taking $\eta_{\rm E} = \eta_{\rm B}$ we have prescribed a particular energy per baryon E/B in the fireball and we can concurrently solve the pressure equilibrium constraint given by Eq. (16) to determine the pressure. Since the pre-equilibrium QGP phase is not observable with hadronic probes, much of the detail of the evolution is lost. As we find, it suffices to use the energy and pressure constraints to determine the properties of the fireball at the time the nuclear collision terminates. We make here the plausible hypothesis[4] that when the collision has terminated (at about 1.5 fm/c in the CM frame), the u, d quarks and gluons have reached their chemical equilibrium, $\gamma_{\rm q} \to 1$, $\gamma_{\rm G} \to 1$. Furthermore, the strange flavor is still far from equilibrium and we choose $\gamma_{\rm s} \simeq 0.15$ appropriate for strange

[4]The finite baryon density and baryon number conservation in the fireball force onto the system a rather large quark density, which is there from the beginning and needs not be produced; gluons are more easily produced than quark pairs and thus presumably their number catches up with the quark number by the time the collision has terminated. Note that in baryon-free central region environments expected at much higher RHIC/LHC energies, the approach to chemical equilibrium can be different.

Table 1: Properties and evolution of different collision systems.

Phase space occupancy	$<s-\bar{s}>=0$ $\lambda_s \equiv 1$	E/B [GeV]				
		2.6 $\eta=1$ Au–Au	4.3 $\eta=1$ Pb–Pb	8.8 η=0.5 S–Pb	8.6 η=0.75 Pb–Pb	8.6 $\eta=1$ Pb–Pb
	T_{th} [GeV]	0.260	0.361	0.410	0.444	0.471
$\gamma_q = 0.2$	λ_q	9.95	3.76	1.78	1.91	2.00
	n_g/B	0.20	0.54	1.55	1.36	1.25
	n_q/B	3.00	3.13	5.12	3.89	3.77
$\gamma_g = 0.2$	$n_{\bar{q}}/B$	0.00	0.13	2.12	0.89	0.77
	$n_{\bar{s}}/B$	0.02	0.06	0.16	0.14	0.13
	P_{th} [GeV/fm^3]	0.46	0.76	0.79	1.12	1.46
$\gamma_s = 0.03$	$\rho_{\rm B}$	3.34	3.30	1.70	2.44	3.18
	S/B	11.8	18.8	40.0	35.8	33.4
	T_{ch} [GeV]	0.212	0.263	0.280	0.304	0.324
$\gamma_q = 1$	λ_q	4.14	2.36	1.49	1.56	1.61
	n_g/B	0.56	1.08	2.50	2.24	2.08
	n_q/B	3.11	3.51	5.16	4.81	4.62
$\gamma_g = 1$	$n_{\bar{q}}/B$	0.11	0.51	2.16	1.81	1.62
	$n_{\bar{s}}/B$	0.05	0.11	0.25	0.22	0.21
	P_{ch} [GeV/fm^3]	0.46	0.76	0.79	1.12	1.46
$\gamma_s = 0.15$	$\rho_{\rm B}$	3.35	3.31	1.80	2.45	3.19
	S/B	12.3	19.7	41.8	37.4	34.9
	γ_s	1	1	0.8	1	1
$\gamma_q = 1$	T_0 [GeV]	0.184	0.215	0.233	0.239	0.255
	λ_q	4.14	2.36	1.49	1.56	1.61
$\gamma_g = 1$	n_g/B	0.56	1.08	2.50	2.25	2.09
	n_q/B	3.11	3.51	5.12	4.81	4.60
	$n_{\bar{q}}/B$	0.11	0.51	2.12	1.81	1.62
$\gamma_s = 0.8$	$n_{\bar{s}}/B$	0.34	0.68	1.27	1.43	1.33
or	P_0 [GeV/fm^3]	0.30	0.41	0.47	0.54	0.71
$\gamma_s = 1$	$\rho_{\rm B}$	2.17	1.80	1.05	1.19	1.56
	S/B	14.5	24.0	49.5	46.5	43.4

quark relaxation time 7 times larger than the light quark one [21]. Because the QGP phase is strangeness neutral we have $\lambda_{\rm s} = 1$. The remaining statistical parameters $T_{\rm ch}$ and $\lambda_{\rm q}$ are now fixed by the EoS and are shown with other interesting properties of the fireball (number of gluons per baryon, number of light quarks and antiquarks per baryon, number of anti-strange quarks per baryon, the pressure in the fireball, baryon density and the entropy per baryon) in the middle section of the table 1 .

After the collision has ended, for times $t \geq 1$ fm/c, but probably also ≤ 3–5 fm/c, we relax the strange quarks to their equilibrium abundance and the temperature drops from $T_{\rm ch}$ to the value T_0. The bottom portion of the table corresponds to this full chemical equilibrium (with exception of the S–W case for which we assume that strange quarks have reached 80% of phase space occupancy as suggested by the experimental results [2, 38]). During the formation of the strangeness flavor there is already evolution of the fireball outside of the collision region and we allow for this by keeping $\lambda_{\rm q} = $ Const. This effectively freezes the entropy content of gluons and light quarks, allowing for significant drop in pressure and some cooling due to conversion of energy into strangeness.

In order to have some understanding of the possible thermal conditions prevailing in the early stages of the collision process, when the thermal equilibrium is reached, we have in the top section of the table 1 selected some reasonable off-chemical equilibrium conditions — we consider 20% occupancy for gluons and light quarks, and 3% for strange quarks and solve the same equations as for $T_{\rm ch}$, and the associated $\lambda_{\rm q}$. There is no change in the pressure, as the dynamical compression is present at this stage of the fireball evolution. But we see here in particular that the temperature $T_{\rm th}$ is considerably higher, since the number of quarks and gluons present is considerably lower.

The columns of table 1 correspond to the cases of specific experimental interest, see top legend, in turn: Au–Au collisions at AGS, possible future Pb–Pb collisions at SPS with 40A GeV, S–Pb at 200A GeV, and for the Pb–Pb collisions at 158A GeV we considered two possible values of stopping, see Eq. (21): $\eta = 0.75$ and $\eta = 1$.

As discussed in section 2, the temperature values shown in the bottom portion of the table are similar to the inverse slopes observed in particle spectra and shown in Fig. 2. Remarkably, the values of temperature T_0 found for the case of $E/B = 8.6$ GeV at $\eta = 0.5 \pm 0.1$ is just 233 MeV, which corresponds nearly exactly to the reported inverse slopes of the WA85 results [27], and $\lambda_{\rm q} = 1.49$ also agrees exactly with the results of our analysis [2], also shown in Fig. 2. Even though there are a number of tacit and explicit parameters (in particular $\eta = 0.5, \alpha_s = 0.6$) which enter this result the degree of the agreement is stunning and encourages us to explore in systematic fashion the variation of the key parameters with the energy content of the fireball.

In Fig. 4 we show, as function of the specific energy content E/B, the expected behavior of temperature T_0, the light quark fugacity $\lambda_{\rm q}$ and entropy per baryon S/B at the time of full chemical equilibration in the QGP fireball. The range of the possible values as function of η is indicated by showing results, for $\eta = 1$ (solid line), 0.5 (dot-dashed line) and 0.25 (dashed line). The experimental bars on the right hand side of the Fig. 4 show for high (8.8 GeV) energy the result of analysis [2] of the WA85 data [27]. The experimental bars on the left hand side of the Fig. 4 (2.6 GeV) are taken from our analysis of the BNL-AGS data [14], but note that in this case we had found $\lambda_{\rm s} = 1.7$ and not $\lambda_{\rm s} = 1$ as would be needed for the QGP interpretation at this low energy. For the BNL-AGS range of energies $E/B = 2.3$–2.6 GeV, we expect $\eta \simeq 0.9$–1 and this is indeed in good agreement with the QGP-based evaluation [14] of the experimental results ($T = 180 \pm 30$ MeV, $\lambda_{\rm q} = 4.8 \pm 0.4$ and $S/B = 13 \pm 1$). We can explain in this analysis the case of S–S collisions which have a lot of flow [3, 39]: we take at $E/B = 9.6$ GeV a stopping fraction $\eta \simeq 0.3 \pm 0.1$ which yields $T_0 \simeq 196 \pm 13$ MeV, in agreement with the experimental results for the inverse slope [40]. The value of $\lambda_{\rm q}$ which

traces the baryon density cannot be so easily estimated in this case, we refer to a study of the possible rapidity dependence of λ_q made recently [39].

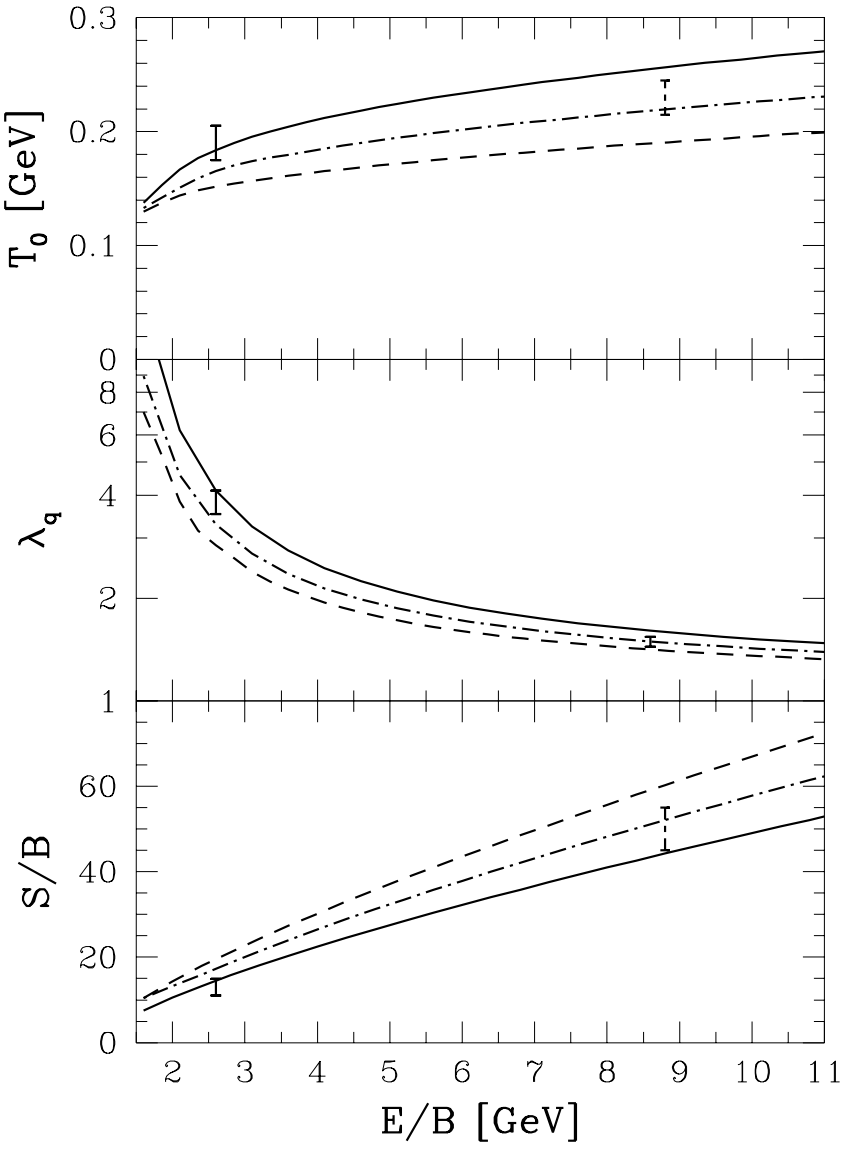

Figure 4: Temperature T_0, light quark fugacity λ_q and entropy per baryon S/B at the time of full chemical equilibration as function of the QGP-fireball energy content E/B. Results for momentum stopping $\eta = 1$ (solid line), 0.5 (dot-dashed line) and 0.25 (dashed line) are shown. See text for comparison with analysis results.

Among the key features in the Fig. 4, we note that, in qualitative terms, the drop in temperature with decreasing energy and stopping is intuitively as expected, and the value of λ_q is relatively insensitive to the stopping power, and also varies little when the energy changes by $\pm 15\%$. This implies that even when different trigger conditions lead to different stopping fractions η_i, the resulting value of λ_q which is determining the strange particle

(baryon/antibaryon) ratios, is rather independent of different trigger conditions. Our analysis shows that λ_q *decreases while* E/B *increases*. This behavior can be argued for by noting that baryon density is higher in the QGP at lower energies. However, note that this intuitive insight was really arising from our belief that the stopping of baryon number decreases as energy of the collision increases, while the result here found occurs irrespective of the change in baryon stopping. This has considerable impact on the behavior of strange particle ratios as function of collision energy (see section 3). Another important result is the rapid rise of specific entropy with the energy content: while at the BNL-AGS energies we find similar entropy contents in the confined and deconfined phases of hadronic matter, at CERN energies we encounter twice as much entropy in the deconfined phase, which leads to a noticeable excess in particle abundances [11]. We turn to discuss this important issue now.

2.7 Entropy and Particle Multiplicity

An important observable of the thermal fireball which allows to cross check the validity of our approach is its entropy content. We recall the first law of thermodynamics in the form:

$$E = TS - PV + \mu_B B\,, \tag{22}$$

which with the relativistic EoS (negligible masses, no dimensioned scale in the interactions):

$$P = \frac{1}{3}\left(\frac{E}{V} - 4\mathcal{B}\right), \tag{23}$$

leads to the simple relation:

$$\frac{S}{B} = \frac{4}{3}\frac{1}{T}\frac{E}{B} - \ln\lambda_B - \frac{4}{3}\frac{\mathcal{B}V}{BT}\,. \tag{24}$$

Note that this equation can only be applied to systems in chemical equilibrium. The two last terms in Eq. (24) are comparatively small compared to the first term. We see that the entropy content can be relatively accurately estimated. For $E/B = 8.8$ GeV and $T = 235$ MeV we find $S/B = 50$ in agreement with other studies [2, 11] and the results shown in the table 1 above. More complete numerical calculations yield the specific entropy at fixed specific energy as function of one statistical parameter, or as shown in Fig. 5, as function of the momentum stopping. In Fig. 5 we show how the entropy per baryon varies as function of stopping for different energies per baryon $E/B = 2.6$ to 10.6 GeV. The experimental bar in lower right corresponds to our analysis of the BNL-AGS results [14], and is in agreement with stopping being greater than 80% if QGP were formed at these energies. The cross in the middle of the figure is indicating the region in which we believe the S–W/Pb system to be (stopping 0.5 ± 0.1, specific entropy as discussed in [2] and just above, see Eq. (24). We note that the solid line, corresponding to the energy content of S–W/Pb collisions, passes right through this region.

This fact that entropy per baryon is primarily dependent on the specific energy content in the fireball offers us the opportunity to explore further the hypothesis which had lead us to determine the relation between the kinematic energy and the fireball energy, see section

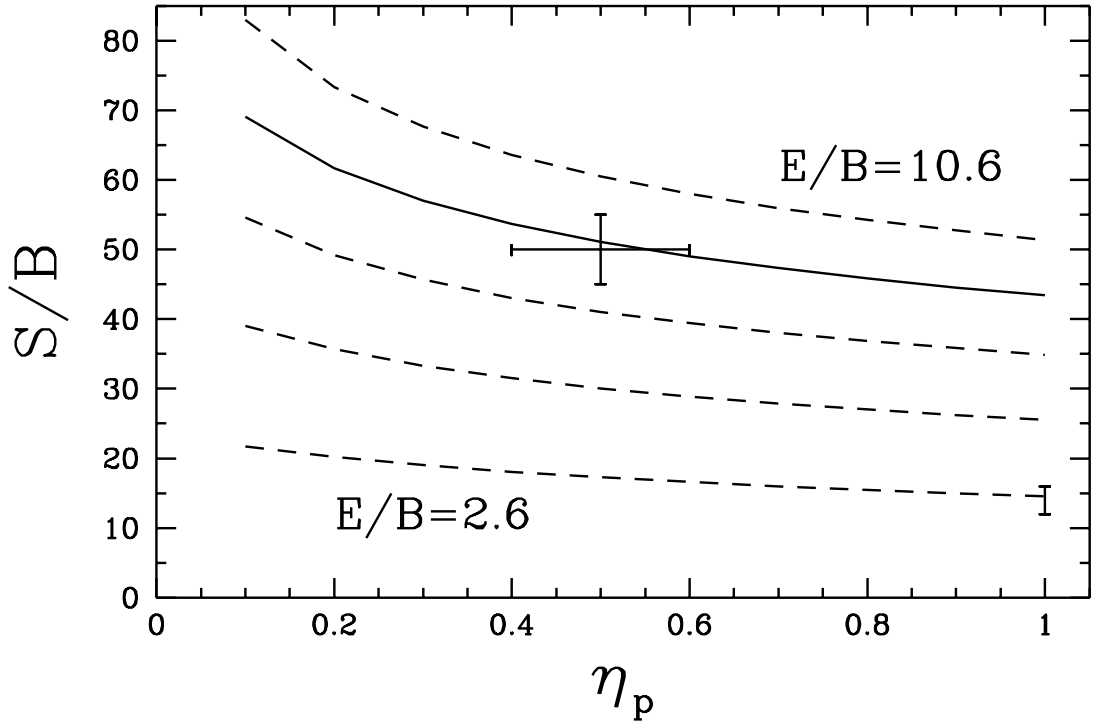

Figure 5: Specific entropy S/B as function of momentum stopping $\eta_{\rm p}$ at given energy content of the QGP-fireball E/B = 2.6, 4.6, 6.6, 8.6, and 10.6 GeV. See text for discussion of the experimental points.

2.4. Should the energy stopping be greater than baryon stopping even by 15%, then the specific energy content would be much more greater, and in Fig. 5 we see that this would be implying a greater momentum stopping $\eta_{\rm p} \to 1$. Since both energy and momentum stopping should increase together this is a possible scenario, and hence we must always remember that the 160–200A GeV collisions as possibly leading to a greater specific energy. Conversely, if we were to assume that energy stopping is smaller by 15% than baryon stopping, this would imply a reduction of the specific energy and as seen in Fig. 5 would require $\eta_{\rm p} \to 0.2$, which is clearly not seen in the experiments. We conclude that either all stopping fractions at CERN-SPS energies are similar or that there is a somewhat smaller baryon stopping. The qualitative results about transverse energy production [41] suggest that we should not consider $\eta_{\rm E} > 0.5$ for 200A GeV S–W/Pb collisions.

The experimentally measurable quantity is not the entropy, but the final state particle multiplicity [11, 15]. A useful observable is the quantity $D_{\rm Q}$:

$$D_{\rm Q}(y) \equiv \frac{\left(\frac{dN^+}{dy} - \frac{dN^-}{dy}\right)}{\left(\frac{dN^+}{dy} + \frac{dN^-}{dy}\right)} \,. \tag{25}$$

Note that in the numerator of $D_{\rm Q}$ the charge of particle pairs produced cancels out and it is effectively a measure of the baryon number; thus in the product $D_{\rm Q}$ with S/B the baryon content cancels, and the result is roughly the entropy content of the final state per final state pion number (denominator of $D_{\rm Q}$). Specifically, $D_{\rm Q} \cdot (S/B) \simeq 3$ [2] for a wide range

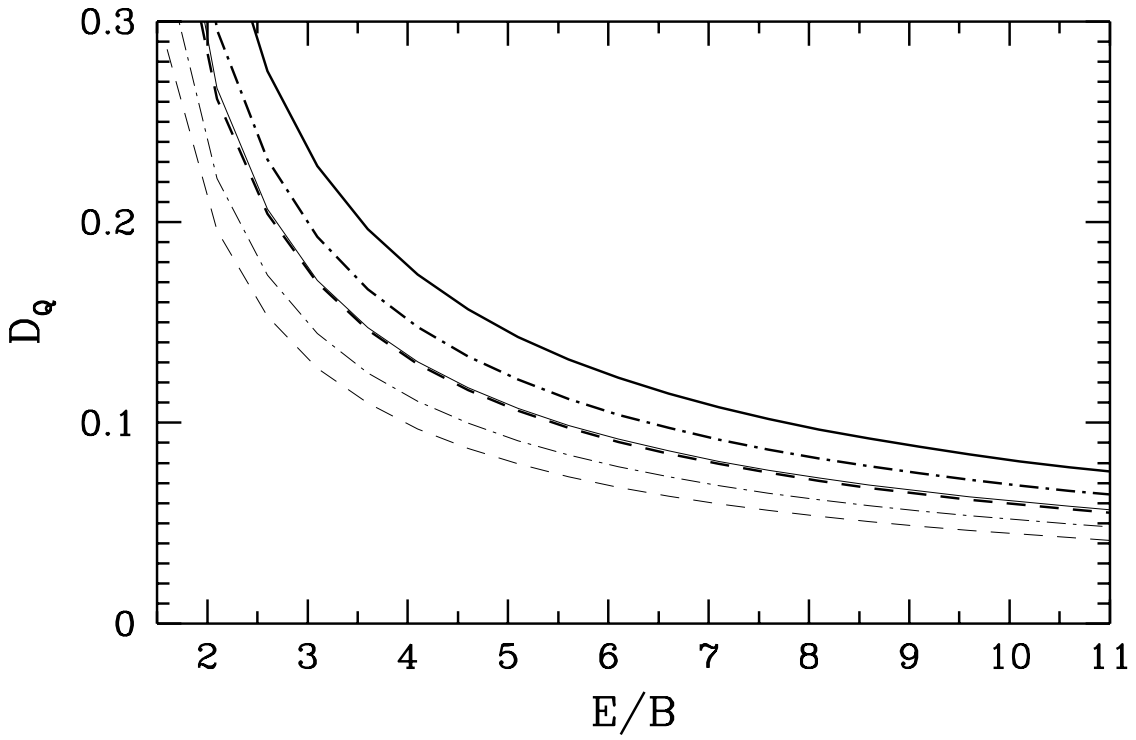

Figure 6: $D_{\rm Q}$ versus E/B. Thick line $D_{\rm Q}\,S/B = 4$, thin line $D_{\rm Q}\,S/B = 3$. $\eta = 1$ (solid line), $\eta = 0.5$ (dot-dashed line) and $\eta = 0.25$ (dashed line).

of $T, \lambda_{\rm q}$ and at $\lambda_{\rm s} = 1$, and taking the population of heavy hadronic resonances emitted from the fireball as expected from a hadronic gas system in chemical equilibrium. However, the hypothesis of the equilibrated hadronic gas as a transient phase is highly inconsistent with the strange particle flow, which suggests no re-equilibration and direct disintegration of the fireball into final state hadrons. If this were the case, the production of heavy meson resonances would be suppressed against the thermal equilibrium expectations. Consequently, the dilution of the number of charged hadrons by decays of heavy neutrals would not occur and we should observe $D^0_{\rm Q} \cdot (S/B) \simeq 4.4$, where the superscript '0' indicates that we did not account for the particle decay in the quantity $D_{\rm Q}$. In Fig. 6 we show as thick lines, using $D_{\rm Q} \cdot (S/B) \simeq 4$, how the observable $D_{\rm Q}$ depends on collision energy. Thin lines are for $D_{\rm Q} \cdot (S/B) \simeq 3$ — the momentum stopping varies between 1 (solid lines), 0.5 (dot dashed) and 0.25 (dashed). Experimentally, in S–Pb collisions the EMU05 collaboration finds $D_{\rm Q} = 0.085 \pm 0.01$, shown at 8.8 GeV in Fig. 6. As the CERN-SPS energy is lowered to 4.3 GeV in CM frame (40A GeV for the projectile) which is presumably accompanied by an increase in stopping to $\eta = 1$, the value of $D_{\rm Q}$ rises and reaches $D_{\rm Q} = 0.16$, nearly twice the S–W/Pb results. We thus see that the widely different specific entropy values shown at the bottom of table 1 become measurable by means of the observable $D_{\rm Q}$ and conclude that $D_{\rm Q}$ is an extraordinarily valuable experimental variable which differentiates structures arising in the collision and from which in particular quantitative information about specific entropy can be gained.

We note in passing that a computation of the confined hadronic gas entropy [2, 11] at the same statistical conditions of the fireball yields only 50% of the QGP-fireball specific entropy value, and thus suggests in view of the observed particle multiplicities that the fireball could not have been just an assembly of confined hadrons.

3 Strange Particles from QGP

3.1 General Remarks

The observable 'strangeness' is more than just one quantity which is enhanced by a factor two or two and a half when one compares usual p–p and p–A with A–A reactions. The interesting aspects of this observable are that certain strange particles are much more enhanced than others, and moreover, the production mechanisms being very different from the usual ones, the behavior of the yields (cross sections) with energy can be expected to be of different nature. A thermal fireball source can emit hadronic particles during its entire evolution. The observable strange particles are: $\mathrm{K}^{\pm}$, $\mathrm{K_S}$, ϕ, Λ, $\overline{\Lambda}$, Ξ^-, $\overline{\Xi^-}$, Ω and $\overline{\Omega}$. We should include here the closely related antiprotons $\bar{p}$, which leads us to consider 11 types of particles. Leaving out an overall normalization factor associated with the reaction volume, and recalling that there is a constraint between the abundance of kaons ($\mathrm{K}^+ + \mathrm{K}^- \simeq 2\mathrm{K}_S$) we have 9 independent normalization parameters describing the yields. These can be redundantly measured with the help of the $36 = 9 \cdot 8/2$ independent particle yield ratios. Aside of the yield normalization parameters, there are in principle 11 different spectral shapes which we above implicitly presumed to be related to each other: The experimental fact that once effects related to particle decays and (transverse) flow are accounted for, the $m_\perp$ spectra are characterized by a common inverse slope parameter, cannot be taken lightly and suggest strongly that the source of all strange particles is indeed thermalized with a common temperature and that a common mechanism governs production of different strange particles.

3.2 Final State Particle Counting

It is easy to propose mechanisms that would largely erase memory of the transient QGP phase. We will not discuss this class of *re-equilibrating* hadronisation pictures [42] of strange particles which seems not to be present at least at CERN-SPS energies [2]. Instead, we shall focus our attention on the alternative that the particles emerge directly from the deconfined phase, be it because of their radiative emission [5], be it because a general rapid and explosive disintegration of the hot fireball occurs in the final stage of its evolution.

The abundance of particles emerging in explosive disintegration or radiated is, according to Eq. (2), determined by the normalization constant:

$$N_j = V \prod_i n_i \,, \qquad n_i = g_i \lambda_i \gamma_i, \tag{26}$$

where it is assumed that the final state particle of type j contains the quark valence components of type i and these are counted using their statistical degeneracy g_i, fugacity

$\lambda_i = \exp(\mu_i/T)$ and the chemical equilibration factor γ_i. V is the emission source volume. Fragmentation of gluons could contribute to the abundance of the valence quarks and has been considered previously [5]. Because it enhances the number of all quarks and the effect is weighted in a similar way for all flavors, and further, since in the ratio of particle abundances a partial cancelation of this effect occurs, this effect is apparently of lesser importance.

Once the factor γ_i accounts for the deviation from the full phase space occupancy of the species i, the chemical potentials for particles and antiparticles are opposite to each other and the particle and antiparticle abundances are related, see Eq. (5). As indicated in Eq. (26), the fugacity of each final state hadronic species is the product of the valence quark fugacities. The abundances of the final state strange particles is gauged by considering the Laplace transform of the phase space distribution of strange particles, which leads to a partition function $\mathcal{Z}_{\rm s}$ like expression (27). The weight of individual components is controlled by the non-equilibrium coefficients $\gamma_{\rm s}$, relative meson and baryon abundance parameters $C^{\rm s}_{\rm B}$, $C^{\rm s}_{\rm M}$ and by the fugacities $\lambda_{\rm q}$, $\lambda_{\rm s}$:

$$\ln \mathcal{Z}_{\rm s} = \frac{VT^3}{2\pi^2}\Big\{(\lambda_{\rm s}\lambda_{\rm q}^{-1}+\lambda_{\rm s}^{-1}\lambda_{\rm q})\gamma_{\rm s}C^{\rm s}_{\rm M}F_K + (\lambda_{\rm s}\lambda_{\rm q}^{2}+\lambda_{\rm s}^{-1}\lambda_{\rm q}^{-2})\gamma_{\rm s}C^{\rm s}_{\rm B}F_Y + (\lambda_{\rm s}^{2}\lambda_{\rm q}+\lambda_{\rm s}^{-2}\lambda_{\rm q}^{-1})\gamma_{\rm s}^2C^{\rm s}_{\rm B}F_\Xi + (\lambda_{\rm s}^{3}+\lambda_{\rm s}^{-3})\gamma_{\rm s}^3C^{\rm s}_{\rm B}F_\Omega\Big\}\ , \tag{27}$$

where the kaon, hyperon, cascade and omega degrees of freedom are included. Here T is the freeze-out temperature. The phase space factors F_i of the strange particles are (with g_i describing the statistical degeneracy):

$$F_i \ = \ \sum_j g_{i_j} W(m_{i_j}/T)\ . \tag{28}$$

In the resonance sums $\sum_j$ all known strange hadrons should be counted. The function $W(x)$ arises from the phase-space integral of the different particle distributions $f(\vec{p})$. For the Boltzmann particle phase space, when the integral includes the entire momentum range, the well known result is found

$$W(x) \equiv (4\pi)^{-1}\int d^3(p/T) f(\vec{p}) = x^2K_2(x)\,, \tag{29}$$

where $x = m/T$ and $K_2(x)$ is the modified Bessel function.

Because the emission volume of the particles is not known, only the ratio

$$R^{\rm s}_{\rm C} = C^{\rm s}_{\rm M}/C^{\rm s}_{\rm B} \tag{30}$$

appears in observables of interest. Note that, only because we are allowing for the possibility of the QGP formation, we must allow for the effect of non-equilibrium hadronisation with $C^{\rm s}_{\rm B,M} \neq 1$ — there is no reason whatsoever to expect that the rapid disintegration of the deconfined state will lead to particle abundances that are associated with chemical equilibrium of the final state. We note that relative abundances of meson and baryons emerging from hadronising QGP are difficult to equilibrate, because processes which convert meson into baryon–antibaryon pairs are relatively slow.

Determination of the freeze-out temperature and the non-equilibrium hadronisation parameter $R^{\rm s}_{\rm C}$ requires that we observe the kaon to (strange) baryon ratios. We will discuss this point below in section 3.4 .

3.3 Strangeness Conservation

There is a strong constraint between the two fugacities λ_q, and λ_s arising from the requirement of strangeness conservation which was discussed at length recently [2]. The manner in which this relation works, depends critically on the nature of the particle source and we shall now explore the meson-baryon off-equilibrium effects. These non-trivial relations between the parameters characterizing the final state are in general difficult to satisfy and the resulting particle distributions are constrained in a way which differs considerably between different reaction scenarios which we have considered in detail: the rapidly disintegrating QGP or the equilibrated HG phase. These two alternatives differ in particular by the value of the strange quark chemical potential μ_s:

1. In a strangeness neutral QGP fireball μ_s is always exactly zero, independent of the prevailing temperature and baryon density, since both s and $\bar{s}$ quarks have the same phase-space size.

2. In any state consisting of locally confined hadronic clusters, μ_s is generally different from zero at finite baryon density, in order to correct the asymmetry introduced in the phase-space size by a finite baryon content.

At non-zero baryon density, that is for $\mu_B \equiv 3\mu_q \neq 0$, there is just one (or perhaps at most a few) special value $\mu_B^0(T)$ for which $\langle s\rangle = \langle\bar{s}\rangle$ at $\mu_s^{HG} = 0$, which condition mimics the QGP. For the case of a conventional HG (Hagedorn type) we have studied these values carefully [10]. For the final state described by Eq. (27), this condition of strangeness conservation takes the simple analytical form [11, 2]:

$$\mu_q^0 = T\cosh^{-1}\left(R_C^s\frac{F_K}{2F_Y} - \gamma_s\frac{F_\Xi}{F_Y}\right), \quad \text{for } \mu_s^{HG} = 0\ . \tag{31}$$

There is at most one non trivial real solution for monotonous arguments of $\cosh^{-1}$, and only when this argument is greater than unity.

Clearly, the observation [2] of $\lambda_s = 1$ ($\mu_s = 0$) is, in view of the accidental nature of this value in the confined phase, a rather strong indication for the direct formation of final state hadrons from a deconfined phase, in which this is the natural value. We note that a further refinement [39] of the original analysis [3] of the S–S system at 200A GeV, which allows for a rapidity dependence of λ_q due to flow further underpins the finding $\lambda_s = 0$. We can thus safely conclude that strange particles produced in 200A GeV Sulphur interactions with diverse targets lead to a particle source which displays a symmetry in phase space size of strange and anti-strange particles. A natural explanation is that such a source is deconfined. It will be very interesting to see, if this behavior is confirmed for the Pb–Pb system and different collision energies.

3.4 Freeze-out Conditions

This is not the place to develop a complete hadronisation model of the QGP fireball — instead we are trying to circumvent the need for a detailed model of hadronisation by introducing a global single parameter R_C^s which will allow to determine the relative ratio of meson

and baryon particle yields. There is a simple way to fix $R_{\rm C}^{\rm s}$: the strangeness conservation condition Eq. (31) must apply to the particle emitted from the fireball, with chemical conditions determined by the source: thus for each value of $\mu_{\rm q}$ and $T = T_{\rm f}$ there is a corresponding value of $R_{\rm C}^{\rm s}$ for which the strangeness remains balanced. $R_{\rm C}^{\rm s} = 1$ would almost always lead to asymmetric emission of the strange particles and thus in all cases to the formation of a final $\bar{s}$ or s strangelett nuggets, except in the unusual condition that the QGP disintegration occurs when the plasma and HG phase-spaces for $\bar{s}$ or s particle-carriers are the same. In any event, it is extremely instructive to study how the values of the so defined $R_{\rm C}^{\rm s}$ depend on the properties of the fireball.

We use here the experimentally motivated $\gamma_{\rm s} = 0.7$, though the deviation from unity is of little numerical importance in present argument. Since the (multi-)strange (anti)baryon particle ratios have led to $\lambda_{\rm q} = 1.48$ and $\lambda_{\rm s} = 1.03$ we use the QGP freeze-out value $\lambda_{\rm s} = 1$ and set $\lambda_{\rm q}$ to three values in Fig. 7. The solid line is for $\lambda_{\rm q} = 1.5$, an appropriate choice for the case of S–W collisions at 200A GeV, (when $\lambda_{\rm s} = 1$). The short dashed curve is for the choice $\lambda_{\rm q} = 1.6$ which is as large as $\lambda_{\rm q}$ will get for the case of Pb–Pb 160A GeV collisions; we see that we are finding rather narrow range of $R_{\rm C}^{\rm s}$ for each given freeze-out temperature. The long dashed curve is for $\lambda_{\rm q} = 2.5$, the value which our model calculations suggest for the 40A GeV collisions (see table 1).

The value $R_{\rm C}^{\rm s} = 1$ is found for $T \simeq 200$ MeV at $\lambda_{\rm q} \simeq 1.5$–$1.6$. For lower temperatures we have $R_{\rm C}^{\rm s} < 1$, which implies that the size of the strange baryon phase space needs to be increased compared to thermal equilibrium (or the strange meson phase space needs to be reduced) in order to allow a balance between strange and anti-strange quarks in emission from the QGP fireball.

As noted in passing above, a description of hadronisation using $R_{\rm C}^{\rm s} = 1$ leads to a s, $\bar{s}$ asymmetry in the developing fireball. The question is which of the two evolution options: the off-equilibrium particle emission, or strangeness distillation, is consistent with the experimental data. This can be decided considering a physical observable which is primarily sensitive to the parameter $R_{\rm C}^{\rm s}$, and to a lesser degree to the other thermal model parameters. We choose to study the kaon to hyperon abundance ratio, both for all phase space and at fixed $m_\perp$. In the latter case we have:

$$R_{\rm K}|_{m_\perp} \equiv \left.\frac{K_{\rm s}^0}{\Lambda + \Sigma^0}\right|_{m_\perp} \simeq \frac{R_{\rm C}^{\rm s}}{8}\,\frac{\lambda_{\rm s}/\lambda_{\rm d} + \lambda_{\rm d}/\lambda_{\rm s}}{\lambda_{\rm s}\lambda_{\rm u}\lambda_{\rm d}}\,. \tag{32}$$

We made a preliminary study of this relation in [10], which is valid when resonance decay contributions cancel. To account here in necessary detail for the resonance decay influence, we have incorporated the decay pattern of all listed resonances numerically. The thick lines in Fig. 8 give $R_{\rm K}|_{m_\perp}$ at fixed $m_\perp$ as function of $R_{\rm C}^{\rm s}$, see Eq. (32). We include the descendants of strong and weak decays in order to facilitate comparison below with experimental data. We assumed that the distribution of parent particles for kaons and hyperons is according to the thermal equilibrium condition evaluated at temperature as given in the Fig. 7. The values of $\lambda_{\rm q} = 1.5$, 1.6, 2.5 and line conventions are the same as used in that figure. The thin lines in Fig. 8 give results covering the full phase space. Since the kaon mass is much smaller than hyperon mass, this ratio $R_{\rm K}|_{\rm tot}$ is considerably greater than $R_{\rm K}|_{m_\perp}$, and hence we use logarithmic scale to display both $R_{\rm K}$. We see in particular that in order to have

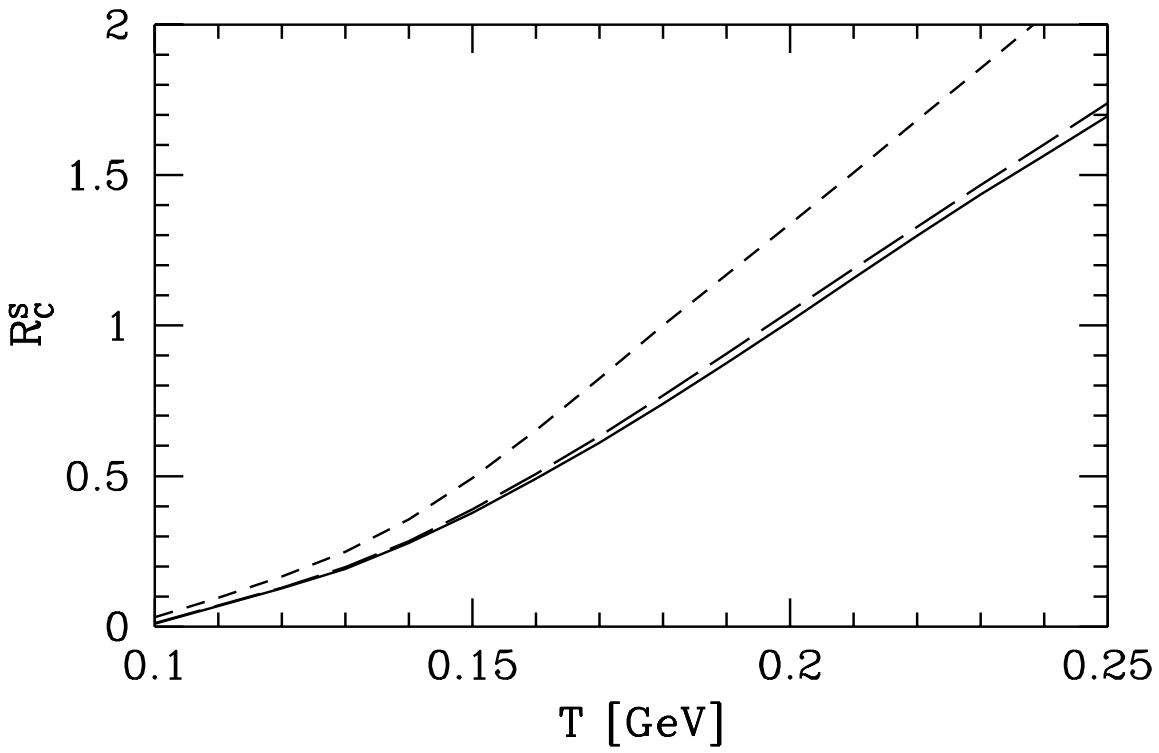

Figure 7: Strangeness neutrality line: $R^{\rm s}_{\rm C}$ versus freeze-out temperature for $\lambda_{\rm q} = 1.5$ (solid line), $\lambda_{\rm q} = 1.6$ (long dashed line) and $\lambda_{\rm q} = 2.5$ (short dashed line).

HG-equilibrated yield of kaons and hyperons for fixed $m_\perp$, i.e. when $R^{\rm s}_{\rm C} = 1$, we would have to find experimentally $R_{\rm K}|_{m_\perp} \simeq 0.3$ in the S–W/Pb and/or Pb–Pb collisions.

There is no officially reported value for the $R_{\rm K}$ ratio. However, collaboration WA85 has presented [43] a figure which shows for largely overlapping $1.1 < m_\perp < 2.6$ GeV the yields of Λ, $\overline{\Lambda}$ and $K_{\rm S}$ for the central rapidity region $2.5 < y < 3$. No cascading corrections was applied to these results. Using graphic methods we obtained $R_{\rm K}|_{m_\perp} = 0.11 \pm 0.02$. This implies a far off-HG-equilibrium result $R^{\rm s}_{\rm C} = 0.4$ as shown in Fig. 8, and thus as seen in Fig. 7 a freeze-out temperature $T_{\rm f} \simeq 150$ MeV. The possibility that $R^{\rm s}_{\rm C} \simeq 1$ ($R_{\rm K}|_{m_\perp} \simeq 0.3$) is experimentally completely excluded. The factor $R^{\rm s}_{\rm C} \neq 1$ confirms the expectation that the reactions which change the number of baryons (baryon-antibaryon formation by mesons) are relatively slow in the confined phase [44], or that all strange particles originate directly from the QGP fireball. In any case we conclude that the observed value $R^{\rm s}_{\rm C} = 0.4$ allows to fix the freeze-out conditions, here in particular $T_{\rm f} = 150$ MeV.

The final issue is how, from the value $R^{\rm s}_{\rm C} = 0.4$, we can infer the values of the abundance constants $C^{\rm s}_{\rm M}$ and $C^{\rm s}_{\rm B}$ which (see Eqs. (27, 30)) express the relative strange meson and baryon production abundance to the thermal equilibrium values. If we argue that the strange meson abundance, akin to total meson abundance is enhanced by factor two (i.e. $C^{\rm s}_{\rm M} = 2$) as we found studying the entropy enhancement, then the conclusion would be that the strange baryons are enhanced (against their tiny HG equilibrium abundance at $T_{\rm f} = 150$ MeV) by factor $C^{\rm s}_{\rm B} = 5$. It is clear from this observation that strange baryons and antibaryons are

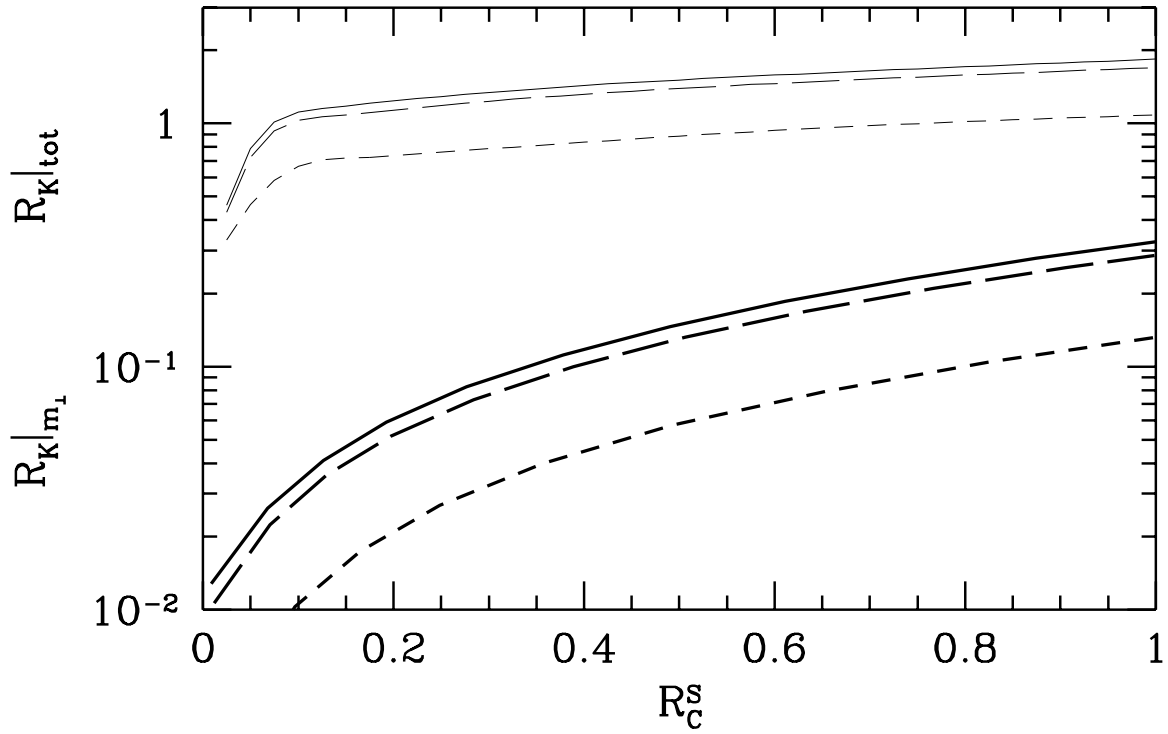

Figure 8: Thick lines: $R_{\rm K}|_{m_\perp}$, thin lines: $R_{\rm K}|_{\rm tot}$ as function of $R_{\rm C}^{\rm s}$ for $\lambda_{\rm q} = 1.5$ (solid line), $\lambda_{\rm q} = 1.6$ (long dashed line) and $\lambda_{\rm q} = 2.5$ (short dashed line).

thus the key to the study of the deconfined state. We now turn to study these particle yields.

3.5 Strange Baryons and Antibaryons

The ratios of strange antibaryons to strange baryons *of same particle type*: $R_\Lambda = \overline{\Lambda}/\Lambda$, $R_\Xi = \overline{\Xi}/\Xi$ and $R_\Omega = \overline{\Omega}/\Omega$, are in our approach simple functions of the quark fugacities and have been discussed at length recently [2, 6]. In view of our current work we can predict the behavior of these ratios as function of energy. Using the results for $\lambda_{\rm q}$ shown in Fig. 4, we show in Fig. 9 these three ratios. Since we assume $\lambda_{\rm s} = 1$, we have $R_\Omega = \lambda_{\rm s}^{-6} = 1$, but since some re-equilibration is to be expected towards the HG behavior $\lambda_{\rm s} > 1$, we expect $\lambda_{\rm s} = 1 + \epsilon$, with ϵ small, and thus for this ratio $R_\Omega = 1 - 6\epsilon < 1$. A further non negligible correction which has been discussed at length in Ref. [2] is due to the isospin asymmetry: in the heavy Pb–Pb collisions it will be necessary to account for d–u asymmetry which is as large as 15%, and which favors the abundance of particles with d-quark content over those with u-quark content. This impacts here in particular the ratio R_Ξ, since there are no light quarks contributing to R_Ω and the ratio R_Λ is u-d symmetric.

We now study the ratios between antibaryons with different strange quark content. These are dependent on the degree of the strangeness saturation reached, and we shall take in this study $\gamma_{\rm s} = 1$ assuming relatively large, long-lived system created in the collisions of largest available nuclei. In the Figs. 10–12 we show three ratios and for each ratio three results:

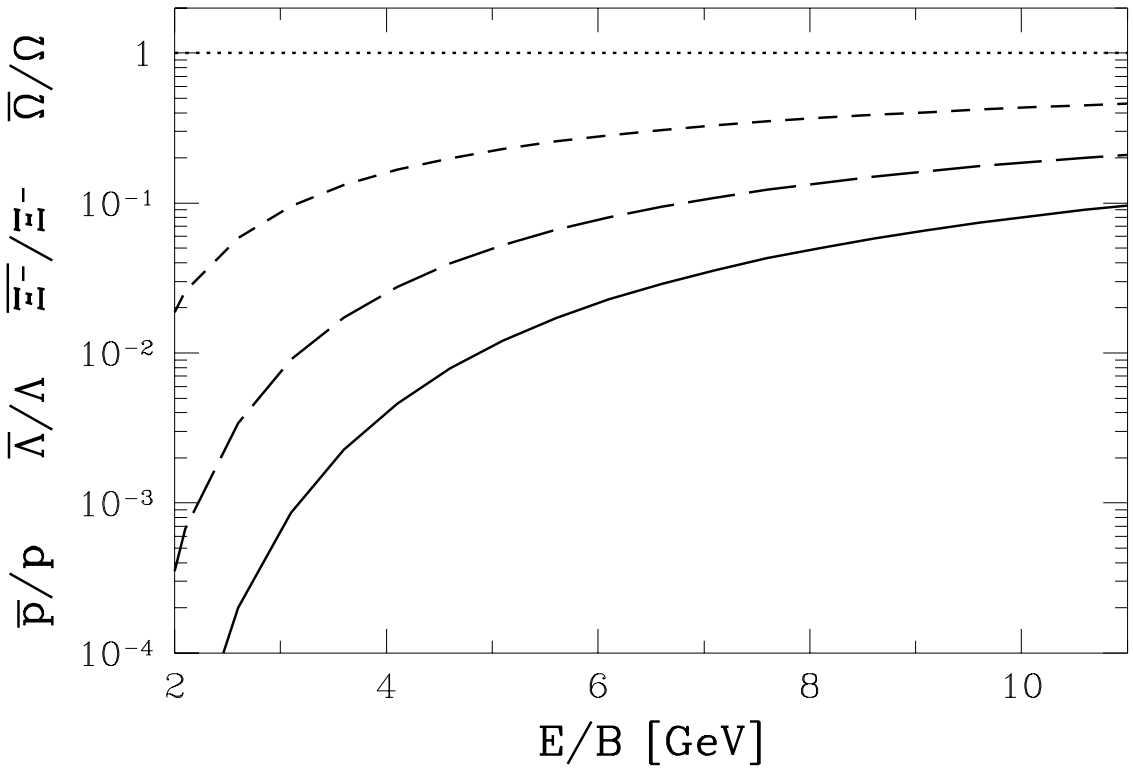

Figure 9: Antibaryon to baryon abundance ratios as function of energy per baryon E/B in a QGP-fireball: $R_{\rm N} = \bar{p}/p$ (solid line), $R_\Lambda = \overline{\Lambda}/\Lambda$ (long-dashed line), $R_\Xi = \overline{\Xi}/\Xi$ (short-dashed line) and $R_\Omega = \overline{\Omega}/\Omega$ (dotted line)

solid lines depicts the result for the full phase space coverage, short dashed line for particles with $p_\perp \geq 1$ GeV and long dashed line for particles with $m_\perp \geq 1.7$ GeV. In Fig. 10 we show the ratio $\overline{\Lambda}/\bar{p}$, in Fig. 11 the ratio $\overline{\Xi^-}/\overline{\Lambda}$ and in Fig. 12 the ratio $\overline{\Omega}/\overline{\Xi^-}$. Because $\lambda_{\rm q}$ rises with decreasing E/B, see Fig. 4, we encounter overall the remarkable behavior that these three ratios increase as the collision energy is reduced.

The behavior shown in Figs. 10–12 may be of considerable importance, if our expectations are confirmed that in reaction models in which QGP is not assumed and the particles are made in a sequence of microscopic collisions these ratios *do increase* with the collision energy, reflecting in this behavior the behavior of the reaction cross section observed in p–p reactions. If this behavior is found at low energies and it matches at some energy at which a jump to the here presented yields, then the QGP behavior obtained here is truly the smoking gun type evidence for the formation of the deconfined phase. Furthermore, it would be a rather easy task to determine the transition energy to QGP by merely seeking where these ratios peak as function of E/B.

As a final step in this discussion we present now the analysis of the available and very recent WA85 Ω/Ξ^- production ratio [45] and the $\overline{\Lambda}/\bar{p}$ ratio of the NA35 collaboration obtained for the S–Au system at 200A GeV [46]. Fig. 13 shows a comparison of our ab initio calculation and the pertinent experimental results. We use the same cuts on the range of $p_\perp$ as in the

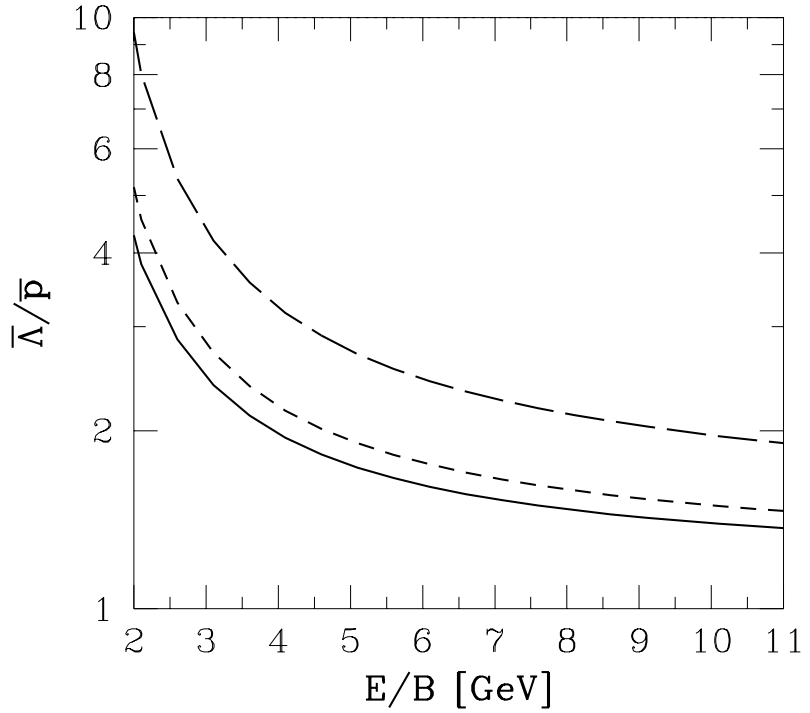

Figure 10: Strange antibaryon ratio $\overline{\Lambda}/\overline{p}$, as function of E/B in a QGP-fireball; solid lines are for full phase space coverage, short dashed line for particles with $p_\perp \geq 1$ GeV and long dashed line for particles with $m_\perp \geq 1.7$ GeV.

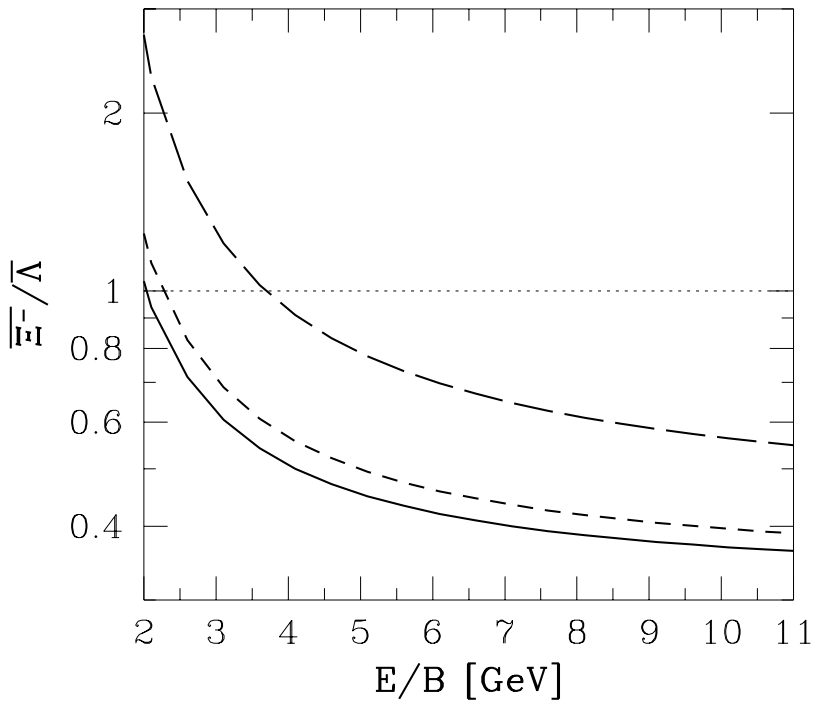

Figure 11: Strange antibaryon ratio $\overline{\Xi^-}/\overline{\Lambda}$ with the same conventions as in Fig. 10.

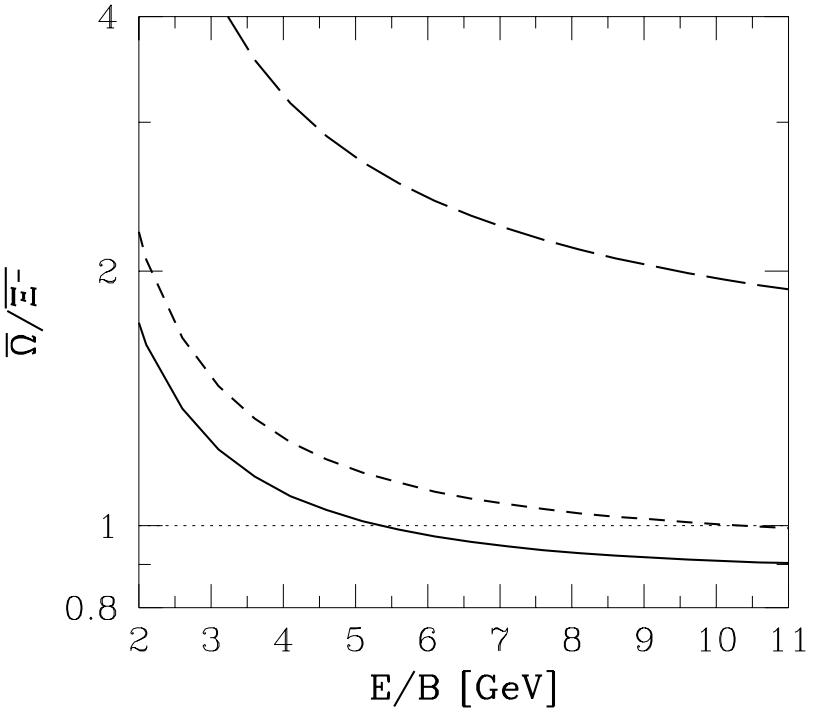

Figure 12: Strange antibaryon ratio $\overline{\Omega}/\overline{\Xi^-}$ with the same conventions as in Fig. 10.

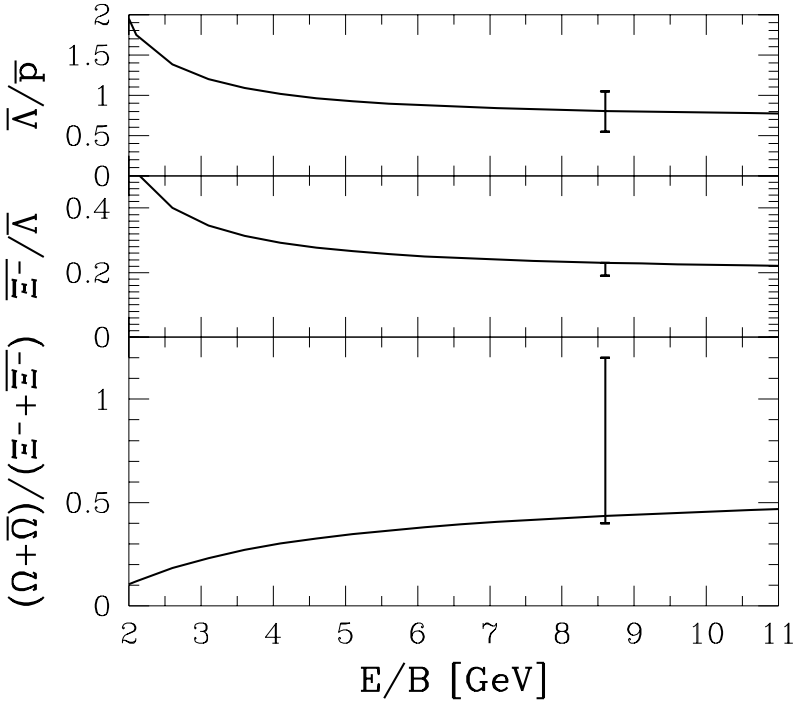

Figure 13: Strange antibaryon ratios for S–W/Pb collisions as function of E/B in a QGP-fireball: $\overline{\Lambda}/\overline{p}$ (full phase space), $\overline{\Xi^-}/\overline{\Lambda}$ for $p_\perp > 1.2$ GeV and $(\overline{\Omega}+\Omega)/(\overline{\Xi^-}+\Xi^-)$ for $p_\perp > 1.6$ GeV; experimental results shown are from experiments NA35, WA85.

experiment: the experimental points show the results $\overline{\Lambda}/\bar{p} \simeq 0.8 \pm 0.25$ (NA35) for full phase space, $\overline{\Xi^-}/\overline{\Lambda} = 0.21 \pm 0.02$ (WA85) for $p_\perp > 1.2$ GeV; and $(\Omega + \overline{\Omega})/(\Xi^- + \overline{\Xi^-}) = 0.8 \pm 0.4$ (WA85) for $p_\perp > 1.6$ GeV. The chosen value of $\gamma_{\rm s} = 0.70$ and $\eta_{\rm p} = 0.5$ brings about good agreement of our model with the precise value of $\overline{\Xi^-}/\overline{\Lambda}$. Fig. 13 shows also the impact of the change of the collision energy on these results, using 50% stopping, rather than $\eta = 1$ used in Figs. 10–12.

Considering that we have computed here everything in an ab initio dynamical model (which as discussed above has some tacit and explicit parameters such as the QCD coupling $\alpha_{\rm s} = 0.6$ etc., chosen to be in agreement with the earlier experimental results) it is remarkable that such a good agreement with the two very recent results could be attained. We can conclude that the fact that the two ratio $\overline{\Lambda}/\bar{p}$ (NA35) and $(\Omega + \overline{\Omega})/(\Xi^- + \overline{\Xi^-})$ (WA85) are satisfactorily explained, provides a very nice confirmation of the consistency of the thermal fireball model.

An interesting question which arises quite often is how the particle and in particular antibaryon yields vary with energy. Eq. (27) allows to determine the absolute particle yields as function of fireball energy. Considerable uncertainty is arising from the off-equilibrium nature of the hadronisation process, which in particular makes it hard to estimate how the different heavy particle resonances are populated, and also, how the abundance factors $C_{\rm B}^{\rm s}$ vary as function of energy. Some of this uncertainties are eliminated when we normalize the yields at an energy, which we take here to be the value $E/B = 2.6$ GeV which is applicable to the BNL-AGS experiments. In Fig. 14 the so normalized yields of antibaryons taking the freeze-out temperature $T = 150$ MeV are shown (we also assume $\gamma_{\rm s} = 1$, $\eta_{\rm p} = 1$ and absence of any re-equilibration after particle emission/production). These yields are rising in qualitatively similar systematic fashion with energy, as would be expected from the microscopic considerations, but the rise of more strange antibaryons is less pronounced, unlike what we would naively have expected. The quantitative point to note is that at BNL-AGS ($E/B = 2.6$ GeV) the yield from a disintegrating QGP-fireball is a factor 100–400 smaller compared to yields at E/B =9 GeV. Since the particle density dN/dy is not that much smaller at the lower energies (recall that the specific entropy, see table 1 , drops only by factor 3.5, implying a reduction in specific multiplicity by a factor 5), it is considerably more difficult at the lower energies to search for antibaryons than it is at higher energies. We should remember that the results presented in Fig. 14 are obtained assuming formation of the QGP-fireball and same freeze-out and hadronisation conditions for all energies shown.

4 Summary and Conclusions

The key issue of interest to us is the identification of the deconfined quark-gluon plasma state in relativistic nuclear collisions. We have shown [2] in recent work that many features of strange particle production results obtained at 200A GeV, are consistent with the QGP hypothesis; and we have argued that the conventional reaction picture involving a fireball made of confined hadrons is for a number of reasons incompatible with these experimental results. We felt that in order to ascertain the possibility that indeed the QGP phase is

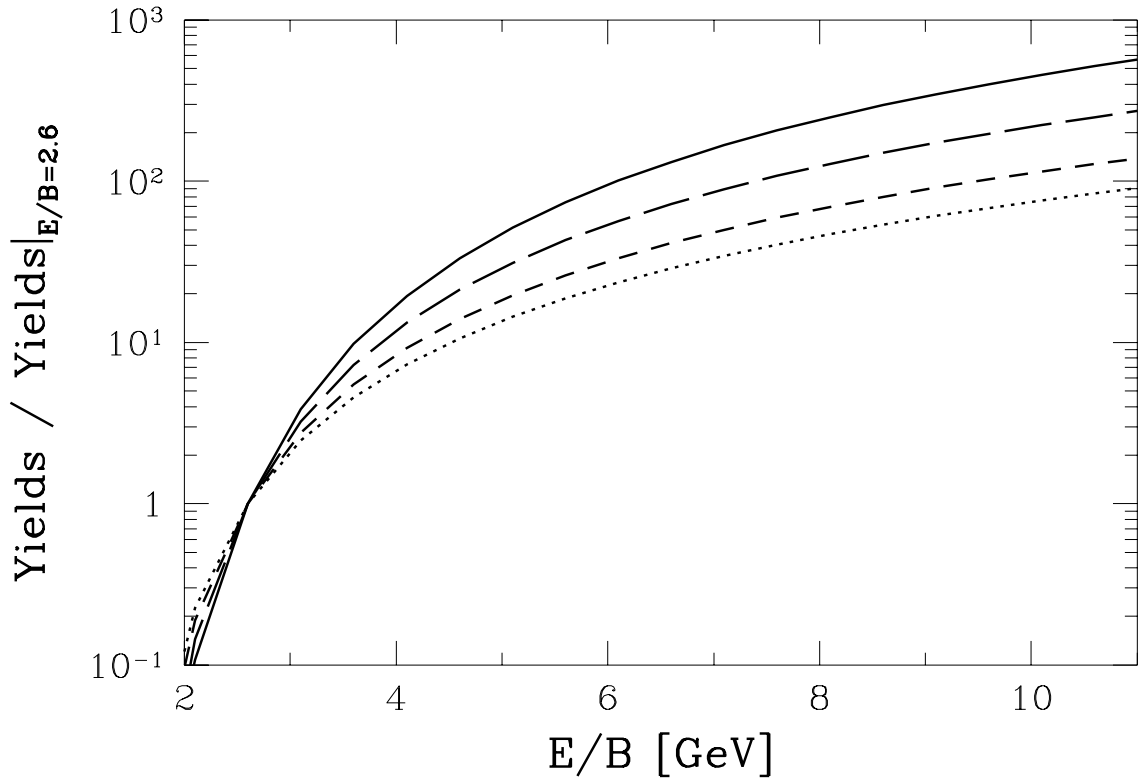

Figure 14: Relative antibaryon yields as function of E/B in a QGP-fireball. $\overline{p}$ (solid line), $\overline{\Lambda}$ (long-dashed line) $\overline{\Xi^-}$ (short-dashed line) and $\overline{\Omega}$ (dotted line), all normalized to their respective yields at $E/B = 2.6$ GeV .

already formed at 200A GeV a more systematic exploration as function of collision energy of these observables would be needed — conclusions drawn from one set of experimental conditions suffer from the possibility that some coincidental and unknown features in the reaction mechanisms could lead to the observed properties. It is highly unlikely that this would remain the case, should a key feature of the experiment be varied.

Variation of the number of participating nucleons has in the QGP reaction picture the considerable disadvantage that we reduce the size of the deconfined region, which even in the case of Pb–Pb reactions, is not very large. This very likely will reduce the lifespan of the deconfined state, and the key reaction measure, the stopping 'friction' is reduced in such a case as well. All these effects make an interpretation of the data with varying the number of participants, in terms of the same reaction model, exceedingly difficult, if not impossible. Against this drawback, the study of the particle production with change in the reaction energy (measurement of excitation functions) appears to be the best approach, which preserves the maximum attainable size and lifespan of the hypothetical deconfined region, while minimizing the change in the stopping, in particular if one is operating in the energy domain in which for the largest available nuclei the stopping is nearly complete. Furthermore, at some low energy, we must reach the conditions of the normal hadron cascade

interaction, and thus be able to describe the results reliably in terms of established cross sections.

Thus our primary objective in this work was to establish the systematic behavior of the antibaryon yields as the energy and stopping of the colliding large nuclei vary, and to determine how the freeze-out conditions of these particles can be determined. This is necessary since the experimental results suggest that while the thermal (kinetic) equilibrium is established, the chemical (particle abundance) equilibrium in the processes governing final state particle freeze-out is largely not achieved. We thus developed a model which relates the energy content of the fireball to the collision energy and the stopping friction. In order to relate the energy to the statistical properties of the fireball which in our approach controls the particle yields we had to use EoS of the deconfined matter, and in particular to account for the impact of QCD-interactions on the properties of the QGP, see section 2.3. We have then shown how the study of kaon to hyperon ratios allows to determine the meson–baryon chemical non-equilibrium parameter. We found that while the entropy production suggests a meson yield which is about twice that of thermal freeze-out yield, the baryon abundance is five times greater than the small thermal freeze-out abundance.

We believe that the thermal equilibrium approach should not be advanced in the context of A–A collisions as being just an economical, but otherwise approximate and highly limited method. Actually, one can argue that this is a more appropriate approach compared to microscopic dynamical (cascade) models, pending a better understanding of the elementary soft particle and entropy producing [26] hadronic processes. In the A–A reactions there is no reason to expect that 'cascades' of p–p type interactions, which are, as matter of principle, even less understood, lead to adequate understanding of soft particles in nuclear collisions.

We have used a simple model which allows to determine, in a systematic fashion, the thermal conditions reached in high density deconfined matter generated in heavy ion collisions. It is based on the observation that during the collision the compression of the quark-gluon matter can proceed until the internal pressure succeeds in stopping further impact compression. In this picture we worked far from chemical quark-gluon equilibrium, but always assumed that the thermal equilibrium is reached rapidly, even on the scale of the nuclear collision time, which is believed to be $\simeq 1$ fm/c given the geometric size of the nuclei and the Lorenz contraction factors.

Motivated by the absence of chemical particle abundance equilibrium, natural for a thermal HG in the final state, we employ a picture of particle production which involves rapid disintegration of the QGP-fireball [6]. Central to the particle abundances are then the chemical properties of the QGP-fireball and we have discussed these comprehensively as function of collision energy and stopping in section 2.6. We have shown that the thermal conditions we find at the end of strangeness chemical equilibration in the fireball, see bottom of table 1 , are in good agreement with our expectations derived from particle yields seen in S–Pb/W collisions. To carry through this program we needed to make a reasonable choice of remaining parameters: in particular stopping $\eta = 50\%$ — about equal for baryon number, energy and pressure; perturbative EoS of particular form we discussed at length in section 2.3. Given these assumptions and parameters, we were able to study, the current strange particle data at 200A GeV and have reached a very satisfactory agreement with experiment as is shown in Fig. 10.

With this encouragement, we have computed in a systematic fashion the behavior of strange particle (kaon, baryon and antibaryon) yields assuming conditions likely to occur in Pb–Pb interactions (e.g. full stopping and $\gamma_s = 1$). It is most interesting that these results show patterns of behavior which could indeed be unique for the QGP type of fireballs — in particular, the relative yields of strange antibaryons (see Figs. 10 – 12) lead to greater ratios occurring at smaller collision energies, down to very low energies, where in models involving cascading type reactions such ratios would be so small that their measurement would be difficult. We are persuaded that this pattern of behavior could not occur for normal confined matter, where the rise in cross sections with energy dominates particle yields whenever these are not arising from collective phenomena such as is a deconfined QGP phase.

A much discussed question [8, 9, 10] has been whether current strange particle data are consistent with the fully equilibrated hadronic gas (HG) picture of hot hadronic matter. The motivation for such a hypothesis emanates from the observed rapid thermalization: given that we do not understand the mechanisms of thermalization, one could equally argue for the 'a priori' presence of fully equilibrated (thermal and chemical) HG phase. We do not believe that the chemical and thermal equilibration are due to same physical processes, and thus while allowing thermal equilibrium we maintain the possibility in our analysis that chemical equilibrium develops slowly and not completely during the reaction. The results presented here support this point of view.

We stress that our description of particle production is based on collective mechanisms (QGP-fireball) and is thus intrinsically different from microscopic approaches, in particular when these are based on a hadronic cascade picture. Such models generally exploit specific data and/or extrapolations and assumptions about individual hadronic reactions and their cross sections. If the true underlying thermalization processes are different (as is likely) from those used in current microscopic approaches, and are indeed much faster than cascades suggest, the whole representation of the collision evolution in these microscopic approaches needs to be reviewed — in this perspective our thermal approach, already advocated for the p–p reactions [24] maybe seen as an experimentally well motivated hypothesis. We note that no alternative model to the here developed rapidly hadronising QGP has been proposed which could generate both strangeness abundance and multi-strange antibaryon enhancement. For example the description in terms of the dual parton model DPM, [47], which introduces a number of parameters to enhance strangeness and strange antibaryons, arrives at a considerably smaller relative abundance $\overline{\Omega}/\overline{\Xi}$.

Some of our results, though presented in great numerical detail, could suffer from considerable systematic errors, in particular when overall absolute yield normalization is discussed. For example, to determine the freeze-out conditions we need to determine the kaon yield after all heavy resonances have decayed. We employed all known tabulated resonances (and hence probably not all), and we adopted the statistical spin/isospin factors not always established. Furthermore, there is the influence of the large resonance width which allows that these states are formed at energy below the resonance mass. There is also the possibility that some resonances alter their properties (particle width, mass) in dense matter. All these effects may have significant impact on the relation we have established between kaon to hyperon ratio and thus on the freeze-out conditions, and off-equilibrium properties, which in turn impacts the individual particle yield. The presence of these effects and uncertainties

is also behind our omission from this discussion of the $\phi(\bar{s}s)$-meson, which participates and benefits from the general strangeness enhancement effects, but which is difficult to describe with the precision that is needed.

Fortunately, these systematic uncertainties have very small impact on the strange antibaryon ratios, in particular when these are considered at fixed, high $m_\perp$, and we firmly believe, in view of the results we have obtained here, that such data provide the best hadronic signatures, and diagnostic tools, of the deconfined matter. We recall the large ratios in the QGP-fireball reaction picture, such as $\overline{\Xi}/\overline{\Lambda}$ which we have found at relatively small energies — in microscopic models and near to $\overline{\Xi}$ production threshold in p–p interaction this ratio is very small. This lets us expect that there will be a peak in the relative $\overline{\Xi}/\overline{\Lambda}$ yield as function of collision energy which will provide an interesting possibility to identify the energy at which collective production of strange antibaryons is first encountered. At this energy we should also encounter for the first time the other features of the QGP phase: strangeness production enhancement, strange phase space saturation ($\gamma_{\rm s} \to 1$), entropy enhancement (particle multiplicity enhancement), pattern of strange antibaryon flow showing $\lambda_{\rm s} = 1$.

Acknowledgment

J.R. acknowledges partial support by DOE, grant DE-FG03-95ER40937 .

References

[1] M. Kataja, J. Letessier, P.V. Ruuskanen and A. Tounsi, Z. Physik C **55**, 153 (1992).

[2] J. Letessier, A. Tounsi, U. Heinz, J. Sollfrank and J. Rafelski, Phys. Rev. D **51**, 3408 (1995).

[3] J. Sollfrank, M. Gaździcki, U. Heinz and J. Rafelski, Z. Physik C **61**, (1994).

[4] J. Rafelski and R. Hagedorn, in: *Statistical Mechanics of Quarks and Hadrons*, edited by H. Satz, North Holland, Amsterdam 1981, pp. 253–272;
J. Rafelski, in: *Workshop on Future Relativistic Heavy Ion Experiments*, edited by R. Bock and R. Stock, GSI-Yellow Report 81-6, Darmstadt 1981, pp. 282–324;
J. Rafelski, Phys. Rep. **88**, 331 (1982).

[5] J. Rafelski and M. Danos, *Phys. Lett.* B **192**, 432 (1987); Phys. Rev. D **27**, 671 (1983).

[6] J. Rafelski, Phys. Lett. B **262**, 333 (1991);
J. Rafelski, Nucl. Phys. A **544**, 279c (1992).

[7] J. Letessier, J. Rafelski and A. Tounsi, Phys. Lett. B **292**, 427 (1992).

[8] J. Cleymans and H. Satz, Z. Phys. C **57**, 135 (1993).

[9] J.Cleymans, K. Redlich, H. Satz and E. Suhonen, Z. Physik C **58**, 347 (1993).

[10] J. Letessier, J. Rafelski and A. Tounsi, Phys. Lett. B **321**, 394 (1994).

[11] J. Rafelski, J. Letessier and A. Tounsi, in *Proceedings of the XXVI International Conference on High Energy Physics*, Dallas, Texas, 1992, AIP-Conference Proceedings No 272, p. 983, edited by J.R. Sanford;
J. Letessier, A. Tounsi, U. Heinz, J. Sollfrank and J. Rafelski, Phys. Rev. Lett. **70**, 3530 (1993).

[12] See contributions in *Hot Hadronic Matter*, Proceedings of NATO-ARW held in Divonne, France, June 1994, Plenum Press, New York 1995, edited by J. Letessier, H.H. Gutbrod and J. Rafelski.

[13] M. Gaździcki, in [17, 26].

[14] J. Rafelski and M. Danos Phys. Rev. C **50**, 1684 (1994);
J. Letessier, J. Rafelski and A. Tounsi, Phys. Lett. B **328**, 499 (1994);
J. Stachel et al., in [26] and private communication.

[15] J. Letessier, J. Rafelski and A. Tounsi, Phys. Rev. C **50**, 406 (1994);
J. Rafelski, J. Letessier and A. Tounsi, Acta. Phys. Pol. A **85**, 699 (1993).

[16] P. Koch, B. Müller and J. Rafelski, Phys. Rep. C **142**, 167 (1986); and references therein.

[17] *Strangeness in Hadronic Matter: S'95* Proceedings of Tucson workshop, January 1995, American Institute of Physics Proceedings Series Vol. 340, 1995, edited by J. Rafelski, *in press.*

[18] J. Rafelski and B. Müller, Phys. Rev. Lett. **48**, 1066 (1982); **56**, 2334E (1986).

[19] T. Biro and J. Zimanyi, Phys. Lett B **113**, 6 (1982); *Nucl. Phys.* A **395**, 525 (1983).

[20] P. Koch and J. Rafelski, Nucl. Phys. A **444**, 678 (1985).

[21] N. Bilić, J. Cleymans, I. Dadić and D. Hislop, *Gluon Decay for Strangeness Production in Quark-Gluon Plasma*, University of Cape Town *Preprint*, August 1994, Phys. Rev. C (in press); and references therein.

[22] P. Foka and the NA35 Collaboration; M. Gaździcki and the NA35 Collaboration, in [17].

[23] J.D. Bjorken, Phys. Rev. D **27**, 140 (1983).

[24] H. Grote, R. Hagedorn and J. Ranft, *Particle Spectra*, CERN black report (1970).

[25] J. Rafelski, H. Rafelski and M. Danos Phys. Lett. B **294**, 131 (1992).

[26] See contributions in *Hot Hadronic Matter*, Proceedings of NATO-ARW held in Divonne, France, June 1994, Plenum Press, New York 1995, edited by J. Letessier, H.H. Gutbrod and J. Rafelski.

[27] WA85 collaboration presentations in [17]; see also:
D. Evans et al. (WA85 collaboration), Nucl. Phys. A **566**, 225c (1994);
S. Abatzis et al. (WA85 collaboration), Phys. Lett. B **259**, 508 (1991);
S. Abatzis et al. (WA85 collaboration), Phys. Lett. B **270**, 123 (1991).

[28] R. Santo et al. (WA80 collaboration), Nucl. Phys. A **566**, 61c (1994).

[29] T. Blum, L. Kärkkäinen, D. Toussaint, S. Gottlieb, Phys. Rev. D **51**, 5153 (1995)

[30] E. Schnedermann, J. Sollfrank and U. Heinz, *Fireball Spectra*, in: *Particle Production in Highly Excited Matter*, edited by H.H. Gutbrod and J. Rafelski, NATO Physics series Vol. B **303**, Plenum Press, New York, 1993, p. 175.

[31] A. Schnabel and J. Rafelski, Phys. Lett. B **207**, 6 (1988); and
in *Proceedings of the 3rd Conference on the Intersection between Particle and Nuclear Physics*, Rockport, 1988, G. Bunce, ed., AIP Proceedings Series No. 176, p. 1068, New York, l988.

[32] P. Koch, B. Müller and J. Rafelski, Z. Physik A **324**, 453 (1986).

[33] J. Rafelski, *On the Trail of QGP: Strange Antibaryons in Nuclear Collisions*, in: *Particle Production in Highly Excited Matter*, edited by H.H. Gutbrod and J. Rafelski, NATO Physics series Vol. B **303**, 529 (1993), Plenum Press, New York; and references therein.

[34] B. Kämpfer, O.V. Pavlenko, A. Peshier and G. Soff, Phys. Lett. B **337**, 235 (1994).

[35] B. Kämpfer, O.V. Pavlenko, A. Peshier and G. Soff, in [17].

[36] J. Letessier, J. Rafelski and A. Tounsi, Phys. Lett. B **333**, 484 (1994).

[37] S.R. de Groot, W.A. van Leeuwen, Ch.G. van Weert, *Relativistic Kinetic Theory,* North Holland, Amsterdam, 1980.

[38] J. Letessier, J. Rafelski and A. Tounsi, Phys. Lett. B **323**, 393 (1994).

[39] C. Slotta, J. Sollfrank and U. Heinz, in [17].

[40] The NA35 collaboration has studied the inverse slopes of particles:
for strange particles see: T. Alber et al., Z. Phys. C **64**, 195 (1994);
for protons and pions see J. Beachler et al., Phys. Rev. Lett. **72**, 1419 (1994);
for antiprotons see: T. Alber et al., preprint IKF-HENPG/5-95, submitted to Phys. Lett. B and [46].

[41] I. Otterlund, *Physics of Relativistic Nuclear Collisions*, in: *Particle Production in Highly Excited Matter*, edited by H.H. Gutbrod and J. Rafelski, NATO Physics series Vol. B **303**, Plenum Press, New York, 1993, p. 57;
S.P. Sorensen et al. *Nuclear Stopping Power*, in: *Proc. XXI Int. Symposium on Multiparticle Dynamics 1991*, World Scientific, Singapore, 1992.

[42] H.W. Barz, B.L. Friman, J. Knoll and H. Schulz, Nucl. Phys. A **484**, 661 (1988) and Nucl. Phys. A **519**, 831 (1990).

[43] D. Evans for the WA85 collaboration, in [17], see Fig. 3; and private communication.

[44] P. Koch and J. Rafelski, Nuc. Phys. A **444**, 678 (1985).

[45] F. Antinori, in [17];
S. Abatzis et al. (WA85 collaboration), Phys. Lett. B **316**, 615 (1993); Phys. Lett. B **347**, 158 (1995).

[46] J. Günther for the NA35 collaboration, to appear in proceedings of QM'95, Monterey, January 1995 (edited by A. Poskanzer et al.); and private communication.

[47] A. Capella, *Strangeness Enhancement in Heavy Ion Collisions* Preprint LPTHE Orsay 94-113; and references therein.